HHS Public Access

Author manuscript

*Neuron*. Author manuscript; available in PMC 2024 April 05.

Published in final edited form as:

*Neuron*. 2023 April 05; 111(7): 1104–1117.e6. doi:10.1016/j.neuron.2022.12.033.

# Ventral tegmental area astrocytes modulate cocaine reward by tonically releasing GABA

**Junhua Yang**[1], **Jianan Chen**[1], **Yongqing Liu**[1], **Kevin Hong Chen**[1], **Jay M. Baraban**[2], **Zhaozhu Qiu**[1,2,3,*]

[1]Department of Physiology, Johns Hopkins University School of Medicine, Baltimore, MD 21205, USA

[2]Solomon H. Snyder Department of Neuroscience, Johns Hopkins University School of Medicine, Baltimore, MD 21205, USA

[3]Lead contact

## Summary

Addictive drugs increase ventral tegmental area (VTA) dopamine (DA) neuron activity through distinct cellular mechanisms, one of which involves disinhibition of DA neurons by inhibiting local GABA neurons. How drugs regulate VTA GABA neuron activity and drive addictive behaviors remain poorly understood. Here, we show that astrocytes control VTA GABA neuron activity in cocaine reward via tonic inhibition in mice. Repeated cocaine exposure potentiates astrocytic tonic GABA release through volume-regulated anion channels (VRACs) and augments tonic inhibition of VTA GABA neurons, thus downregulating their activities and disinhibiting nucleus accumbens (NAc) projecting DA neurons. Attenuation of tonic inhibition by either deleting *Swell1(Lrrc8a)*, the obligatory subunit of VRACs, in VTA astrocytes or disrupting δ subunit of $GABA_A$ receptors in VTA GABA neurons reduces cocaine-evoked changes in neuron activity, locomotion, and reward behaviors in mice. Together, our findings reveal the critical role of astrocytes in regulating the VTA local circuit and cocaine reward.

## eTOC blurb

Yang et al. report that astrocytes in VTA release GABA through the volume-regulated anion channel Swell1 to regulate the activity of VTA GABA and dopamine neurons and modulate cocaine-induced locomotor and reward behaviors in mice.

*Corresponding author: zhaozhu@jhmi.edu.

Author contributions

J.Y. initiated the project, performed all electrophysiological recordings and *in situ* hybridization. J.Y. and J.C. performed cell culture, viral injection, immunostainings, and behavior assays. Y.L. and K.H.C. designed and generated the AAV constructs for *in vivo* CRISPR/Cas9. Results were analyzed and interpreted by J.Y., J.C., Y.L., K.H.C., and Z.Q. J.B. provided critical reagents and edited the manuscript. J.Y. and Z.Q. designed the study and wrote the paper with input from all authors.

Declaration of Interests

The authors declare that they have no competing interests.

## Graphical Abstract

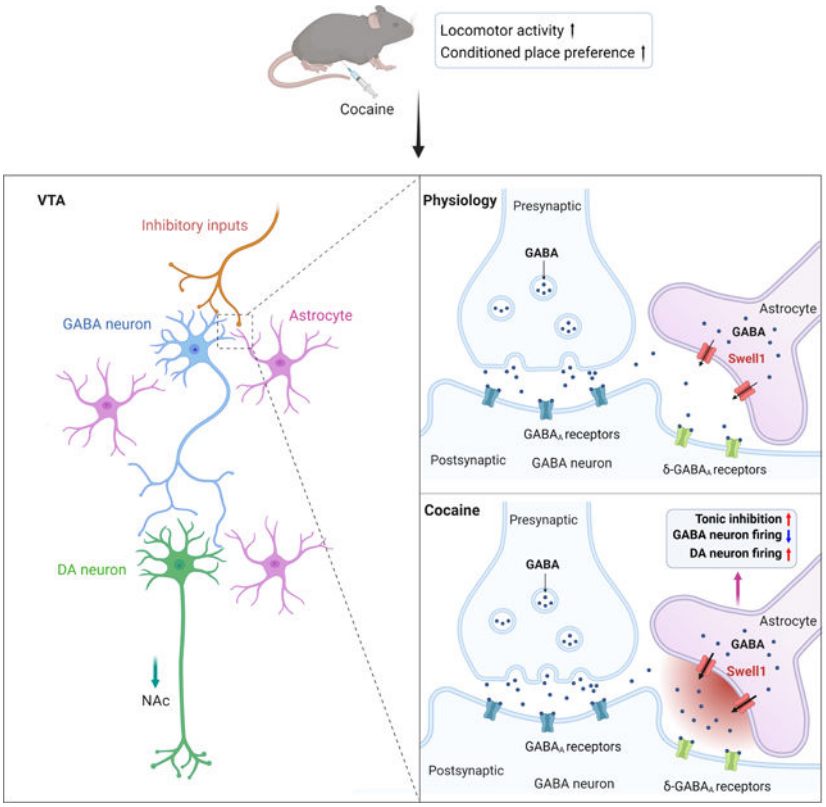


### Keywords

Cocaine reward; astrocytes; tonic inhibition; volume-regulated anion channel; δ subunit of $GABA_A$Rs; addiction

## Introduction

Addictive drugs are known to hijack the mesolimbic dopaminergic system to increase dopaminergic signaling from the midbrain VTA to the nucleus accumbens (NAc) in the ventral striatum [1,2]. How drugs enhance VTA DA neuron activity to cause excessive DA release has been extensively studied. A well-defined mechanism is the potentiation of excitatory synaptic inputs onto DA neurons [3,4]. Moreover, drug-evoked inhibition of VTA GABAergic inhibitory neurons [5–8], which provide strong inhibition directly onto VTA DA neurons [9,10], has also been reported, and results in net disinhibition of DA neurons and increased DA release. In addition to neurons, the VTA is a heterogeneous structure that contains astrocytes, the most abundant glial cells which tile the entire central nervous system and play diverse functions in health and disease. However, the role of astrocytes in mediating the effect of drugs is not well understood.

GABA-mediated tonic inhibition is generated by the binding of ambient GABA to extrasynaptic $GABA_A$Rs, often containing a α5 or δ subunit, that results in a persistent

inhibitory action [11,12]. Due to its sustained nature, tonic inhibition critically modulates neuronal excitability, neural circuit function, and animal behavior [12–14]. While the synaptic release of GABA from neurons is thought to mediate phasic inhibition, astrocyte-derived GABA is proposed to be a major contributor to tonic inhibition [15]. However, the mechanism underlying tonic GABA release from astrocytes is still controversial. Interestingly, recent evidence has revealed that VRACs or Swell1 (also known as Lrrc8a, Leucine-rich repeat containing family 8a) channels [16,17], which play a critical role in cell volume regulation upon osmotic swelling [18], also function as GABA-releasing channels in human cell lines [19] and pancreatic β cells [20]. This raises the possibility that Swell1 channels mediate GABA release from astrocytes and contribute to tonic inhibition. However, the potential involvement of astrocytic *Swell1* in tonic GABA release and in controlling VTA neuron activity in response to drugs of abuse has not been determined.

In this study, we discover that cocaine reduces VTA GABA neuron activity by increasing tonic inhibition through Swell1-dependent GABA release from astrocytes. Reducing tonic inhibition onto VTA GABA neurons via cell-type-specific genetic approaches modulates VTA GABA and DA neuron activity and addiction-related behaviors. Therefore, we identify a novel mechanism for cocaine reward involving a previously unappreciated role for astrocytes and reveal a potential therapeutic strategy of targeting astrocytic Swell1 channels to alleviate addictive behaviors.

## Results

### Cell-type-specific examination of tonic GABA inhibition onto VTA neurons

Tonic inhibition has been widely reported in different mouse brain regions including the VTA [21]. To determine the role of tonic inhibition in drug addiction, we first sought to measure the tonic GABA currents in VTA GABA and DA neurons under physiological conditions. VTA GABAergic inhibitory neurons were identified with a nuclear-localized mCherry using Gad2-T2a-NLS-mCherry (Gad2-mCherry) mice [22] (Fig. 1A) in which mCherry expression is directed by the endogenous *Gad2* promoter/enhancer elements. VTA DA neurons projecting to the NAc, especially the medial shell, drive drug seeking and usage or mediate psychostimulant effects of drugs [23–25]. To specifically label NAc medial shell-projecting DA neurons ($DA_{NAc}$), we injected green fluorescent retrobeads into the NAc medial shell (Fig. 1A). Consistent with previous findings [26,27], we observed that more than 80% of bead-labeled neurons in the VTA are tyrosine hydroxylase (TH)-immunopositive DA neurons, and they were located predominantly in the medial VTA (mVTA) (Fig. 1B, C and Fig. S1A–D). We performed whole-cell patch-clamp recordings on labeled cells in the mVTA and recorded tonic GABA currents in the presence of action potential and ionotropic glutamate receptor blockers (Fig. 1D–F). Tonic GABA currents were measured by recording the change in holding current at −70 mV upon application of $GABA_AR$ antagonist bicuculline (BIC; 100 μM) (Fig. 1D, E). We observed relatively small tonic GABA currents that were of similar amplitude in both VTA GABA and $DA_{NAc}$ neurons (Fig. 1D, E). δ subunit-containing $GABA_A$ receptors (δ-$GABA_A$Rs) have been shown to be expressed in VTA neurons [28,29]. To test whether δ-$GABA_A$Rs are required for tonic inhibition in VTA GABA and $DA_{NAc}$ neurons, we crossed the *Gad2-mCherry* line to mice

lacking the δ subunit (*Gabrd* KO) [30], injected the retrobeads into NAc medial shell, and recorded tonic GABA currents of VTA neurons (Fig. 1A). Compared to control mice, tonic GABA currents of both VTA GABA and $DA_{NAc}$ neurons were dramatically reduced in *Gabrd* KO mice (Fig. 1D, E). These data suggest that tonic inhibition of VTA neurons is mediated by extrasynaptic δ-$GABA_A$Rs.

## GABA-permeable Swell1 channel in VTA astrocytes mediates tonic GABA release

We next investigated the cellular and molecular mechanism underlying tonic GABA release in VTA. Previous studies suggested that astrocytes release tonic GABA in the cerebellum and thalamus through Bestrophin 1 (Best1) [15,31], a $Ca^{2+}$-activated chloride channel [32]. However, the permeability of GABA through the Best1 channel remains controversial [33,34]. Moreover, Best1 expression in VTA astrocytes is very low [35], suggesting that astrocytic GABA release may be mediated by a different mechanism. Indeed, Swell1-containing VRAC is a strong candidate since it has been reported to transport GABA in cell lines [19]. To determine the GABA permeability of VRAC in astrocytes and examine whether VRAC-mediated GABA efflux from astrocytes can be detected by neighboring cells, we adopted the sniffer-patch technique as a sensitive functional bioassay for GABA [15]. As illustrated in Fig. S2A, we performed double whole-cell patch-clamp recordings of an astrocyte, as the source cell, and the adjacent HEK293T cell transfected with the α6, β3, and δ subunits of the $GABA_A$Rs (green fluorescent protein [GFP]-expressing), as the sensor cell. $GABA_A$Rs that include the δ subunit are highly sensitive to low levels of GABA and have relatively little desensitization [36]. It has been suggested that GABA in astrocytes could reach the mM range [31], so we added 5 mM GABA to the pipette solution. After the whole-cell configuration was formed, the intracellular hypertonic solution activated VRAC activity in control source cells as indicated by the developing inward current (Fig. S2B). At the same time, we observed an inward current in the sensor cells, which can be washed away (Fig. S2B) or blocked by BIC (data not shown), indicating that GABA efflux via astrocytic VRAC can be detected by neighboring sensor cells. To quantify the amount of astrocytic GABA release, we normalized the $GABA_A$ currents to maximal receptor activation by direct bath application of 5-mM GABA (Fig. S2B). As expected, intracellular hypertonicity-induced VRAC activity was absent in *Swell1* knockout (KO) source astrocytes (Fig. S2C) which were cultured from brain-specific *Swell1* KO mice by crossing Swell1-floxed mice (*Swell1*$^{F/F}$) with *Nestin-cre* line. Remarkably, GABA efflux from these KO cells was also completely abolished (Fig. S2C, D), demonstrating that astrocytic GABA is released through Swell1-dependent VRACs. Consistent with previous reports [19,20], these data provide strong evidence that GABA permeates through Swell1 channels to mediate GABA release from astrocytes.

To test whether astrocytic Swell1 channels mediate tonic GABA release *in vivo*, we first examined the expression level of *Swell1* in VTA astrocytes by performing RNAscope in situ hybridization (Fig. 2A). We specifically marked astrocytes by crossing *Ai14* reporter mice with *mGFAP-cre* (line 77.6), in which Cre expression is under the control of the mouse glial fibrillary acidic protein (mGFAP) promoter and restricted to astrocytes in the postnatal brain [37]. We observed that VTA astrocytes expressed the highest level of *Swell1* mRNA compared to astrocytes in other brain regions (Fig. 2B, C). To test if *Swell1* plays a role in

tonic GABA release, we measured tonic GABA currents of VTA GABA and $DA_{NAc}$ neurons in control (*Gad2-mCherry; Swell1*$^{F/F}$) and astrocyte-specific *Swell1* knockout (cKO) mice (*Gad2-mCherry; mGFAP-Swell1*$^{-/-}$) (Fig. 2D). We observed that tonic GABA currents of both VTA GABA neurons and $DA_{NAc}$ neurons were largely reduced in cKO mice compared with their littermate controls (Fig. 2E, F). This effect is not due to the unspecific deletion of *Swell1* in neurons since the Cre expression and *Swell1* deletion are highly restricted in astrocytes of VTA in cKO mice (Fig. S3). To specifically delete *Swell1* in VTA astrocytes, we locally microinjected adeno-associated virus expressing Cre recombinase under the control of an astrocyte-specific GFAP promoter (AAV5-GFAP-GFP-Cre) in *Gad2-mCherry; Swell1*$^{F/F}$ mice (Fig. 2G, H). As a control, another cohort of these mice were injected with adeno-associated viruses that only express GFP (AAV5-GFAP-GFP) (Fig. 2G, H). To test the cell-type specificity of this approach, we examined the colocalization of GFP with S100β, an astrocyte-specific marker. As expected, the GFP signals were predominantly expressed in S100β-positive astrocytes (Fig. S4A–D), indicating the selective expression of Cre within VTA astrocytes. The deletion efficiency was also confirmed by a lack of *Swell1* mRNA in Cre-expressing astrocytes using RNAscope (Fig. 2I, J). Using this approach, we recorded the impact of *Swell1* deletion in VTA astrocytes on basal tonic inhibition of VTA GABA neurons. Consistent with the results obtained from cKO mice, the basal tonic GABA currents of VTA GABA neurons were significantly reduced in Cre-expressing mice when compared to controls (Fig. 2K), supporting the requirement of astrocytic *Swell1* for tonic GABA release. It should be noted that a small tonic inhibition current remains following *Swell1* deletion, suggesting other mechanisms or another cellular source may exist. Together, Swell1 is a GABA-permeable channel that mediates tonic GABA release from astrocytes and contributes to tonic inhibition in the VTA.

## Chronic cocaine exposure increases tonic GABA currents in VTA GABA neurons but not $DA_{NAc}$ neurons

Addictive drugs elicit synaptic plasticity that reshapes limbic circuit function and drives drug-induced behaviors [1,2,38]. Therefore, we proceeded to test whether tonic inhibition of VTA GABA and $DA_{NAc}$ neurons is modulated by cocaine, a highly addictive drug that evokes synaptic plasticity at both excitatory and inhibitory synapses of the mesolimbic system [39,40]. To examine the effect of cocaine on tonic inhibition of VTA neurons, we bilaterally injected retrobeads into the NAc medial shell (Fig. 3A). 2 weeks after retrobead injection, we treated mice with saline or cocaine [15 mg/kg intraperitoneally (i.p.), one injection per day] for 5 days [6,41] (Fig. 3A). 24 hours after the last injection, we sacrificed the mice, prepared midbrain slices, and performed whole-cell patch-clamp recordings to measure tonic GABA currents (Fig. 3A). Interestingly, compared to saline treatment, cocaine exposure evoked a significant increase in tonic GABA currents in VTA GABA neurons (Fig. 3B). However, tonic inhibition of $DA_{NAc}$ neurons was similar following saline or cocaine injections (Fig. 3C). Moreover, a single injection of cocaine did not significantly change tonic GABA currents on VTA GABA neurons as measured 1 day later (Fig. S5), suggesting that chronic but not acute cocaine treatment was required to evoke tonic GABA release. Tonic inhibition results from the activation of extrasynaptic $GABA_A$ receptors by extracellular, or “ambient” GABA that diffuses throughout the extracellular space [11]. In addition to GABA, there is ambient glutamate in the extracellular space

which activates extrasynaptic N-methyl-D-aspartate receptors (NMDARs) [42]. We have recently shown that Swell1-dependent VRAC mediates glutamate release from astrocytes in the hippocampus, contributing to the ambient glutamate level[43]. Since glutamate exerts functional counteracting effects of GABA on neurons, we explored whether cocaine exposure affects the ambient glutamate levels as well. We recorded tonic NMDAR currents in the presence of action potential and $GABA_A$ receptor blockers in mice receiving repetitive saline or cocaine injections. Notably, tonic NMDAR currents in either VTA GABA or $DA_{NAc}$ neurons were not changed by cocaine treatment (Fig. 3D, E). These data demonstrate that cocaine evokes not only cell-type- but also neurotransmitter-specific changes in VTA.

With its sustained nature, tonic inhibition exerts a powerful modulatory influence on neural network activity in many brain regions [12–14]. Therefore, we hypothesize that cocaine-evoked potentiation of tonic GABA inhibition onto VTA GABA neurons may dampen their activity, which reduces their inhibitory effect on $DA_{NAc}$ neurons. To test this hypothesis, we recorded spontaneous action potential firing of VTA GABA and $DA_{NAc}$ neurons by performing cell-attached patch-clamp recordings (Fig. 3F). In this configuration, a patch electrode is attached to neurons in brain slices without rupturing the cell membrane and changing its activity. In line with our tonic inhibition data, repeated cocaine treatment significantly reduced the spontaneous firing rate of VTA GABA neurons (Fig. 3G). In addition, $DA_{NAc}$ neurons showed an increased firing rate after repeated cocaine treatment relative to saline-treated mice (Fig. 3H), indicating the disinhibition of $DA_{NAc}$ neurons, most likely due to the inhibition of GABA neurons. These neuronal activity changes in response to cocaine were also consistent with previous *in vivo* recording data [6]. To further confirm this idea, we enhanced tonic GABA current by applying THIP (4,5,6,7-tetrahydroisoxazolo[5,4-c]pyridin-3-ol), a specific agonist for δ-$GABA_A$Rs, and evaluated its effects on VTA neuron activity. Application of THIP (5 μM) evoked significantly larger tonic GABA currents in GABA neurons compared to $DA_{NAc}$ neurons, indicating higher δ-$GABA_A$R expression in GABA neurons (Fig. 4A–C). Interestingly, similar to the effects of repeated cocaine administration, THIP perfusion of brain slices reduced the firing frequency of VTA GABA neurons but enhanced the firing activity of $DA_{NAc}$ neurons (Fig. 4D, E), supporting the notion that inhibition of VTA GABA neurons disinhibits DA neurons. Taken together, these findings suggest that cocaine selectively potentiates tonic inhibition of VTA GABA neurons, and reduces GABA neuronal activity, leading to the disinhibition of DA neurons.

## Astrocytic Swell1 channels contribute to cocaine-evoked tonic GABA release and neuronal firing changes

Since we demonstrated that astrocytic Swell1 channels mediate tonic inhibition in VTA under normal conditions, we asked whether the cocaine-evoked increase of tonic inhibition onto VTA GABA neurons is dependent on Swell1. We specifically deleted *Swell1* in VTA astrocytes locally by microinjecting AAV5-GFAP-GFP-Cre in *Gad2-mCherry; Swell1*$^{F/F}$ mice (Fig. 5A). Mice were injected with AAV5GFAP-GFP as control (Fig. 5A). 4 weeks after AAV injection, we treated mice with cocaine for 5 days and recorded the tonic GABA current of VTA GABA neurons (Fig. 5A). Interestingly, cocaine-evoked potentiation of tonic GABA inhibition of VTA GABA neurons was abolished in Cre-expressing mice, while it

remained intact in control mice (Fig. 5B). Therefore, astrocytic Swell1 channel-mediated tonic GABA release contributes to both basal and cocaine-induced tonic inhibition onto VTA GABA neurons. Next, we investigated the effect of *Swell1* deletion in VTA astrocytes on cocaine-induced neuron firing changes. 4 weeks after AAV and retrobeads injections, we repeatedly treated the mice with saline or cocaine and measured the spontaneous firing activity of VTA GABA and $DA_{NAc}$ neurons (Fig. 5C, D). Consistent with the data in shown Fig. 3G, H, in control mice, cocaine exposure inhibited the firing frequency of VTA GABA neurons and increased the firing rates of $DA_{NAc}$ neurons (Fig. 5E–H). In contrast, cocaine-evoked changes in firing rates of both GABA and $DA_{NAc}$ neurons were abolished by astrocytic *Swell1* deletion in the VTA (Fig. 5E–H), indicating that Swell1-mediated tonic inhibition plays a critical role in regulating VTA neuron activity after cocaine treatment.

How does repetitive cocaine injection potentiate tonic inhibition onto VTA GABA neurons? Astrocytes are known to regulate ambient GABA levels by preferentially expressing GAT-3 GABA transporters [44]. Reactive astrogliosis or reduction of astrocytic GAT-3 has been associated with increased tonic inhibition in several neurological disorders, such as Alzheimer's disease [45,46] and stroke [47]. We explored whether cocaine exposure leads to astrogliosis or decreased expression of GAT-3, as less GABA uptake could result in increased tonic inhibition. Reactive astrocytes display hypertrophy of their main processes and increased GFAP expression [48]. We found that VTA astrocytes expressed very little GFAP in saline-injected mice and cocaine did not change the number of GFAP-positive cells (Fig. S6A–C), providing no evidence for reactive astrogliosis after cocaine treatment. Moreover, GAT-3 expression in VTA astrocytes was similar between the saline and cocaine groups (Fig. S6D, E), indicating that enhanced tonic inhibition was not due to reduced GABA uptake. Furthermore, we examined *Swell1* mRNA expression in VTA astrocytes after repeated cocaine treatment and observed no significant changes compared to saline injections (Fig. S6F, G), suggesting that the increased tonic GABA release may not be caused by the upregulation of Swell1 channel expression level. We proposed a few potential mechanisms underlying the enhanced tonic inhibition after cocaine exposure in the discussion section.

## Disruption of VTA astrocytic tonic GABA release blunts cocaine-induced behavioral changes

Since Swell1-mediated tonic GABA release contributes to the disinhibition of VTA DA neurons by cocaine *ex vivo*, we next investigated the *in vivo* relevance of Swell1-mediated tonic inhibition on behavioral responses to cocaine. In rodents, repeated administration of many addictive drugs, including cocaine, produces locomotor sensitization: a progressive and persistent augmentation of drug-induced behavior thought to mimic addiction-related features in humans [49]. $Swell1^{F/F}$ mice were injected bilaterally with AAV5-GFAP-GFP or AAV5-GFAP-GFP-Cre into the VTA (Fig. 6A and Fig. S7A, B). 4 weeks later, mice were injected (i.p.) with saline for 3 days and then cocaine (15 mg/kg, once per day) for 5 days. After each injection, mice were immediately put into the open-field chamber and monitored for 1 hour (Fig. 6A). The locomotion enhancement elicited by cocaine was significantly reduced in Cre-expressing mice when compared to controls (Fig. 6B), indicating that mice with astrocytic *Swell1* deletion in VTA display decreased sensitization to cocaine.

These results suggest that cocaine-induced increase in tonic GABA inhibition contributes to its behavioral effects. Conditioned place preference (CPP) is a widely-used, standard procedure for assessing the rewarding effects of drugs in rodent models [50]. We, therefore, determined whether cocaine-induced CPP was altered in mice that underwent deletion of *Swell1* from VTA astrocytes. 4 weeks after viral injections, mice were conditioned to cocaine (10 mg/kg) in a 6-day unbiased CPP protocol (Fig. 6C). Each group spent about 50% of their exploration time on the drug-paired side during the pre-conditioning test, confirming the unbiased nature of our CPP procedure (Fig. 6D). Remarkably, on the test day, Cre-expressing mice spent significantly less time in the cocaine-paired chamber than control mice (Fig. 6D) suggesting that *Swell1* deletion from VTA astrocytes reduced cocaine reward. These data demonstrate that disruption of VTA astrocytic tonic GABA release attenuates behavioral effects that underlie cocaine addiction.

## Tonic inhibition onto VTA GABA neurons is critical for cellular and behavioral effects of cocaine

To further evaluate the role of tonic inhibition in cocaine-induced behaviors associated with addiction, we tested whether direct removal of tonic inhibition onto VTA GABA neurons by deleting δ-$GABA_A$Rs affects the cellular and behavioral actions of cocaine. To disrupt the *Gabrd* gene selectively in VTA GABA neurons, we applied *in vivo* cell-type-specific CRISPR/Cas9 gene editing technology which has been widely used to study the function of a target gene in adult mice [51,52]. We first generated a mouse line that expresses Cas9-FLAG and EGFP in all GABAergic inhibitory neurons (Fig. 7A, B). We next constructed an AAV vector encoding two different single guide RNAs (sgRNA) (sgGabrd#1 and sgGabrd#2) targeting different exons and a Cre-dependent fluorescent marker (AAV9-DIO-sgGabrd-mCherry) (Fig. 7B, C). As a control, we constructed an AAV vector encoding two non-targeting sgRNAs (AAV9-DIO-sgControl-mCherry) (Fig. 7C). The specificity and transfection efficiency of the AAV9-DIOsgGabrd-mCherry vector were confirmed by the high degree of colocalization of $GFP^+$ and $mCherry^+$ cells: about 85% of virus-infected cells were $GFP^+$ (Fig. 7D, E). In addition, we confirmed the knockdown efficiency by showing that δ subunit immunostaining in $GFP^+$ and $mCherry^+$ GABA neurons of AAV9-DIO-sgGabrd-mCherry injected mice was dramatically reduced compared to mice injected with AAV9-DIO-sgControl-mCherry (Fig. S8A, B). As expected, VTA GABA neurons of AAV-sgGabrd injected mice had much smaller THIP-induced tonic GABA currents than control neurons (Fig. S8C), consistent with a marked reduction of functional δ-$GABA_A$Rs in these neurons. These data confirm that our *in vivo* cell-type-specific CRISPR/Cas9 approach successfully induced the loss of *Gabrd* gene expression in VTA GABA neurons.

Next, we examined the effect of disruption of the *Gabrd* gene on tonic inhibition by patch-clamp recordings of tonic GABA currents in virus-infected VTA GABA neurons. Consistent with the reduced expression of δ subunit in AAV-sgGabrd injected mice, cocaine-evoked potentiation of tonic GABA currents in VTA GABA neurons of these mice were significantly reduced compared to the GABA neurons of AAV-sgControl injected mice (Fig. 7F, G). Furthermore, cocaine lowered the firing rate of VTA GABA neurons in mice injected with AAV-sgControl but not AAV-sgGabrd (Fig. 7H, I), consistent with the large reduction of tonic GABA inhibition onto these cells in AAV-sgGabrd injected mice. We then assessed

the behavioral consequences of *Gabrd* deletion in VTA GABA neurons. AAV-sgGabrd or AAV-sgControl were injected bilaterally into the VTA of Gad-Cas9 mice (Fig. S8D, E). Interestingly, AAV-sgGabrd injected mice showed significantly reduced cocaine-induced locomotor sensitization (Fig. 7J) and CPP (Fig. 7K) compared to AAV-sgControl injected mice. Overall, specific removal of tonic inhibition onto VTA GABA neurons by disrupting the δ subunit of extrasynaptic $GABA_A$Rs mimics the effects observed with deletion of *Swell1* in VTA astrocytes, i.e., it blocks cocaine-induced changes in VTA GABA neuron firing and attenuates cocaine-induced locomotor sensitization and CPP.

## Discussion

Here, we used a multidisciplinary approach combining retrograde tracing, electrophysiology, mouse genetics, and behavioral assays to investigate the cellular and molecular effects of cocaine on VTA circuitry that mediates its addictive effects. Our study revealed a previously unappreciated and critical role for astrocytes and tonic inhibition in behavioral effects of cocaine that are mediated by the limbic system. Specifically, cocaine induces tonic GABA release from VTA astrocytes via Swell1 channels. Swell-1mediated tonic GABA release activates extrasynaptic δ-$GABA_A$Rs on VTA GABA neurons thereby downregulating their activity and leading to the disinhibition of DA neurons (Fig. 8).

It is well accepted that DA neurons are strongly inhibited by local GABA neurons within the VTA and the rostromedial tegmental nucleus [9,53]. Moreover, distant GABAergic inputs predominantly innervate local GABA, but not DA, neurons in the VTA [6,27,54]. Addictive drugs have been shown to increase mesolimbic DA signaling by a variety of mechanisms, including inhibition of VTA GABA neurons [5–7]. Drugs elicit inhibitory effects on GABA neurons via two main pathways: (1) activation of the $G_{i/o}$-coupled GPCR family [55,56] or ionotropic receptors that inhibit neuron firing through postsynaptic hyperpolarization [57]; (2) potentiation of GABA neurotransmission onto VTA GABA neurons [6]. Here, we elucidate a novel mechanism in which cocaine evokes GABA release from astrocytes which then augments tonic inhibition onto VTA GABA neurons leading to the disinhibition of VTA DA neurons. Furthermore, we also show that blocking this mechanism attenuates the locomotor stimulant effect of cocaine and impairs cocaine CPP. Taken together, these findings imply that the ability of cocaine to potentiate GABA release from VTA astrocytes plays a key role in enhancing mesolimbic DA neuron firing and, thereby, promoting its powerful addictive property.

We observed a selective increase of tonic GABA, but not glutamate, effects in the VTA after cocaine treatment (Fig. 3B–E). Several possibilities could explain this substrate selectivity. First, astrocytes may have different concentrations of GABA and glutamate across brain regions. The majority of synapses in the VTA are GABAergic, so astrocytes may take up more GABA than glutamate in this region. Second, astrocytes display a high degree of molecular and functional heterogeneity allowing them to exhibit brain region-specific properties and functions [58–61]. Finally, VRACs are formed by heteromers of Lrrc8 proteins (Lrrc8a-Lrrc8e); Lrrc8a or Swell1 is the obligatory subunit that combines with at least one other Lrrc8 isoform [17,62]. Importantly, Lrrc8 heteromeric complexes exhibit subunit-dependent transport of substrates [19]. Thus, in addition to the intracellular concentrations

of glutamate and GABA, the expression ratio of Lrrc8 channel subunits in heterogeneous astrocyte populations may influence their relative permeability to these transmitters. This type of subunit-dependent permeability could provide a complex yet elegant mechanism for astrocytes to differentially regulate neuronal activity in various neural circuits. By employing cell-type-/brain region-specific disruption of individual Lrrc8 subunits, future investigations will address the differential role of Lrrc8 isoforms in fine-tuning astrocyte-neuron communication.

Another interesting finding in our study is that cocaine evokes an increase of tonic inhibition onto VTA GABA neurons but not $DA_{NAc}$ neurons. This discrepancy may be explained by the differential expression of the δ subunit between these two groups of cells. We found that VTA GABA neurons have higher THIP-induced currents than $DA_{NAc}$ neurons, suggesting increased δ subunit expression in VTA GABA neurons. Accordingly, VTA GABA neurons would be more sensitive to an elevation of extracellular GABA levels after cocaine treatment. Additionally, astrocytes have been shown to not only respond to but also modulate cell-type- or circuit-specific neuronal activity [61,63]. For instance, optogenetic activation of VTA astrocytes selectively regulates the excitation of local GABA neurons to drive avoidance behavior [64]. Thus, it is possible that a subpopulation of VTA astrocytes selectively respond to VTA GABA neuron activity after cocaine exposure and release GABA that, in turn, specifically acts on those GABA neurons.

How does cocaine induce more tonic GABA release from astrocytes? One explanation is that repeated cocaine exposure increases the GABA content of astrocytes. In line with this idea, astrocytes are reported to release more tonic GABA in neurological disorders such as Alzheimer's disease where astrocytes become reactive and have much higher GABA content than in physiological conditions [45,46]. However, we did not observe either reactive astrogliosis or increased GABA immunostaining (an indicator of GABA content) in astrocytes (data not shown), suggesting that astrocytic GABA content may not change after cocaine exposure. However, we cannot fully exclude this possibility because there could be localized GABA increases that our methods are not sensitive enough to detect. While swell1 upregulation has been reported in some diseases [65], we did not find any significant change in astrocytic *Swell1* mRNA expression following cocaine treatment. Despite similar levels of mRNA, it is possible that Swell1 protein levels could be different due to post-translational modification mechanisms. This question will be addressed by developing specific antibodies that detect Swell1 in tissue in the future. Furthermore, in the absence of changes in GABA content or Swell1 expression, increased Swell1 channel activity in response to cocaine could mediate the observed potentiation of astrocytic GABA release. The existence of tight gap junctions and a large $K^+$ conductance mediated by inwardly rectifying potassium channel 4.1 (Kir4.1) [66] make it technically challenging to isolate hypotonicity-activated Swell1 channel currents in astrocytes of brain slices in adult mice. Therefore, alternative approaches to report Swell1 channel activity are needed to address this possibility. Overall, the mechanism by which cocaine increases tonic GABA release from astrocytes via Swell1 remains to be determined.

The AAV strategy employed in this study bears some general caveats that are worth pointing out. First, there is a concern for the usage of AAVs expressing Cre recombinase in mice

carrying a floxed allele to disrupt a targeted gene in astrocytes to examine the astrocyte-selective role in animal behavior [67]. It was reported that although high Cre-mediated gene deletion efficiency was observed in astrocytes, a low level of off-targeted Cre recombinase in neurons might be sufficient to cause excision of floxed genomic sequences, confounding the explanation of experimental consequences. Indeed, we observed a small proportion of Cre expression and *Swell1* deletion in VTA DA neurons (Fig. S4 and S7C, D). Given our previous findings that *Swell1* deletion in hippocampal neurons does not affect synaptic transmission and plasticity, the behavioral phenotypes after using AAVs in Fig. 6 is unlikely due to the low level of unspecific targeting of *Swell1* in neurons. Second, after AAV microinjection in VTA, the viruses not only infect the medial but also other parts of VTA and sometimes adjacent brain regions. This is another general technical limitation when targeting a sub-region of small brain structures under current virus delivery approaches.

Accumulating evidence has shown that astrocytes are involved in the regulation of reward and drugs of abuse [68–71]. For example, astrocyte inflammation within the reward circuitry, as indicated by increased GFAP expression, has been observed in animal models of drug abuse, particularly following chronic opiate treatments [72,73]. Moreover, repeated self-administration of psychostimulants including cocaine cause a long-lasting adaptation in astrocytes, including downregulation of the glutamate transporter and process retraction from synapses, resulting in glutamatergic transmission dysfunction that promotes cue-induced reinstatement of drug-seeking [74–76]. More recently, NAc astrocytes have been shown to respond to dopaminergic signaling and modulate the acute behavioral psychomotor effects of amphetamine by the release of ATP [77]. Our study further extends our understanding of the role of astrocytes in mediating the action of addictive drugs by demonstrating that cocaine impacts VTA neuronal firing by potentiating tonic astrocytic release of GABA. Importantly, blockade of this pathway attenuates canonical behavioral effects of cocaine that are thought to contribute to its addictive potential. Hence, our findings suggest that Swell1 channels in astrocytes and δ-$GABA_A$Rs in GABA neurons are potential novel therapeutic targets for the treatment of addiction.

## STAR★Methods

### Resource availability

**Lead contact—**Further information and requests for resources, reagents, or code should be directed to and will be fulfilled by the lead contact, Zhaozhu Qiu (zhaozhu@jhmi.edu).

**Materials availability—**This study did not generate new unique reagents or mouse lines.

**Data and code availability—**Data reported in this paper are available from the lead contact upon reasonable request.

This paper does not report original codes.

Any additional information required to reanalyze the data reported in this paper is available from the lead contact upon request.

## Experimental model and subject details

**Animals—**All procedures related to animal care and treatment were approved by the Johns Hopkins University Animal Care and Use Committee and met the guidelines of the National Institute of Health Guide for the Care and Use of Laboratory Animals. All animals were group housed in a standard 12 hr light/dark cycle with *ad libitum* access to food and water. Approximately equal numbers of male and female mice were used for all experiments. The following mouse lines (8- to 12-weeks old) were used for the experiments: C57BL/6J (Jackson Laboratory), *mGFAP-cre* (B6.Cg-Tg(Gfap-cre)77.6Mvs/2J; Jackson Laboratory, 024098), *Nestin-cre* (B6.Cg-Tg(Nes-cre)1Kln/; Jackson Laboratory, 003771), *Gad2-T2a-NLS-mCherry* (B6;129S*Gad2tm1.1Ksvo/J*; Jackson Laboratory, 023140), *Gad2-IRES-Cre* (*Gad2tm2(cre)Zjh/J*; Jackson Laboratory, 010802), Rosa26-Cas9 knockin (*Gt(ROSA)26Sor*$^{tm1.1(CAG-cas9*,-EGFP)Fezh}$*/J*; Jackson Laboratory, 024858), and Ai14 (B6;129S6-*Gt(ROSA)26Sor*$^{tm14(CAG-tdTomato)Hze}$/J; Jackson Laboratory, 007908). The homozygous *Swell1*$^{F/F}$ mice were previously described [43] and were maintained in the laboratory. *Gabrd* KO mice were kindly provided from Dr. Jamie Maguire's laboratory at Tufts University.

**Cell culture and transfection—**HEK293T cells were purchased from ATCC and not further authenticated. Cells were maintained in Dulbecco's modified Eagle's medium (DMEM, Gibco) supplemented with 10% fetal bovine serum (FBS, Gibco) and 1% penicillin/streptomycin (P/S) at 37 °C in humidified 95% $CO_2$ incubators. One day before the sniffer patch recording, cells were digested in 0.25% trypsin (Gibco) and plated onto Poly-D-lysine (Sigma) coated 12-mm coverslips. HEK293T cells were co-transfected with cDNA encoding rat α6 (pIRES2-EGFP vector), β3, and δ subunits (gifts of George Richerson, Department of Neurobiology, University of Iowa, Iowa City, USA) of the $GABA_A$Rs by Lipofectamine 2000 (Invitrogen) following the manufacturer's instructions. On the day of sniffer patch, HEK293T cells expressing $GABA_A$Rs were dissociated, triturated, and added onto the coverslips with primary astrocytes.

To culture primary astrocytes, cortices from P0-P1 newborn pups of both male and female were dissected in ice-cold HBSS and digested in 0.25% trypsin at 37 °C for 20 min. Cells were dissociated by triturating 15–20 times in the culture media (MEM supplemented with 10% FBS and 1% P/S) and plated into a culture flask for 7–10 days. The purity of astrocyte cultures was > 95% as routinely confirmed with GFAP immunostaining. For astrocyte recording, cells were digested and plated onto Poly-D-lysine coated coverslips for at least 24 hours before recording.

## Method details

**DNA constructs and virus packaging—**Gabrd target sites for CRISPR/Cas9 were selected by using the CRISPR website (http://crispor.tefor.net/). The target sequences and PAM were as follows; sgGabrd1: 5′- TATGCCCGAAACTTCCGACCAGG-3′, sgGabrd2: 5′- GGCCTAAGGTCTCGTTGGTATGG −3′. Oligonucleotides encoding guide sequences are purchased from Sigma and cloned individually into BbsI fragment of pX458 (Addgene plasmid 48138). MluI-XbaI flanking U6-sgGabrd1 and XbaI-MluI flanking U6-sgGabrd2 sequences were PCR-amplified, respectively

using pX458-sgGabrd as a template and cloned tandemly into MluI-digested pAAV-CAGDIO-mCherry, a gift from Dr. Hiroshi Yamaguchi. Non-targeting control guide sequences were also PCR amplified from pX458 empty vector by using same primer pairs and cloned tandemly into pAAV-CAGDIO-mCherry in the same way. The primers used were as follows; MluI-F: 5′- CGACGCGTGAGGGCCTATTTCCCA −3′, XbaI-R: 5′- GCTCTAGAAAAAAAGCACCGACTC −3′, XbaI-F: 5′- GCTCTAGAGAGGGCCTATTTCCCA −3′, MluI-R: 5′- CGACGCGTAAAAAAGCACCGACTC −3′. pAAV-U6-sgGabrd1-U6-sgGabrd2 CAG DIO mCherry and pAAV-U6-sgControl-U6-sgControl CAG DIO mCherry were packaged into AAV9 by WZ Biosciences Inc at Maryland.

**Stereotaxic surgeries—**All stereotaxic surgeries were conducted under general anesthesia using continuous isoflurane and body temperature was maintained during surgeries. The depth of anesthesia was monitored continuously and adjusted when necessary. Mice were fitted into a stereotaxic apparatus (RWD Life Sciences) with their heads secured by blunt ear bars. For slice electrophysiology and imaging, mice were injected at the age approximately 4–6 weeks. For all other experiments, mice were injected at age 6–8 weeks. For retrograde labeling, mice were injected bilaterally with green/red fluorescent retrobeads (100 nl; LumaFluor) in the NAc medial shell (NAcMsh, bregma: 1.60 mm, lateral: ±0.7 mm, ventral: −4.70 mm) using a 2.5 μl Hamilton syringe (Hamilton) and a syringe pump (Legato 130, Kd Scientific). Beads-injected mice were used for experiments at least two weeks post-surgery. For AAV injection into VTA (bregma: −3.20 mm, lateral: ±0.40 mm, ventral: −4.50 mm), 0.3–0.4 μl of concentrated AAV were bilaterally injected using a 2.5 μl Hamilton syringe with a 33-G needle (Hamilton) and a syringe pump (Legato 130, Kd Scientific) at 100 nl/min. Following AAV microinjections, the injection needle was left in place for at least 10 min prior to slow withdrawal. The viruses used in this study were purchased from Addgene (AAV5.GFAP. eGFP.WPRE.hGH (AAV5-GFAP-GFP)) and the University of North Carolina Vector Core Facility (AAV5-GFAP-GFP-Cre). All AAV viruses were diluted to titers of 1–3 × $10^{12}$ particles $ml^{-1}$. Virus-injected mice were used for experiments at least 4 weeks post-surgery unless otherwise clarified.

## Immunohistochemistry

**Frozen sections:** Anesthetized mice were perfused transcardially with phosphate-buffered saline (PBS), followed by 4% paraformaldehyde (PFA) in PBS. Brains were removed and post-fixed in 4% PFA at 4 °C overnight. After dehydration by 30% sucrose, brains were embedded in OCT (Tissue-Tek) and cut into 30-μm-thick sections on cryostat microtome (Leica). Sections were permeabilized with 0.3% Triton X-100 and 5% BSA in PBS for 45 min at room temperature (RT), washed with PBS three times, blocked in 10% BSA, and incubated with primary antibodies at 4 °C overnight. For $GABA_A$ δ receptor staining, antigen retrieval was performed prior to immunostaining. Primary antibody concentrations: anti-GFAP (mouse, 1:500, eBioscience, 149892–37), anti-GAT-3 (rabbit, 1:500, Millipore, AB1574), anti-TH (mouse, 1:1000, Millipore, MAB318), anti-TH (rabbit, 1:1000, GeneTex, GTX113016), anti-S100β (rabbit, 1:1000, Abcam, ab41548), anti-mCherry (rat, 1:1000, Thermo Scientific, M11217), anti-$GABA_A$ δ receptor (rabbit, 1:500, Alomone Labs, AGA-014), anti-GFP (rabbit, 1:1000, Invitrogen, A11122), anti-GFP

(rat, 1:1000, Nacalai, 04404–84), anti-FLAG (mouse, 1:1000, Sigma, F1804), anti-NeuN (mouse, 1:200, Millipore, MAB377), anti-NeuN (rabbit, 1:500, Cell Signaling, #24307). After washing 3 times with PBS, samples were incubated with Alexa Fluor-conjugated secondary antibodies (1:1000; Invitrogen) for 1h at RT. Fluorescent images were taken using 10x EC Plan Neofluar 0.3 NA, 20x Plan Apochromat 0.8 NA, 40x LD C-Apochromat 1.0 NA oil immersion, or 63x Plan Apochromat 1.4. NA oil immersion objective lens on a confocal laser-scanning microscope (Zeiss LSM900). Laser settings were kept the same within each experiment. Images represent maximum intensity projections of optical sections with a step size of 1.0 μm. Images were processed with ImageJ.

**Acute sections for biocytin labeling:** After the recording, the pipettes were removed slowly, and the slices were fixed overnight with 4% PFA at 4 °C. Slices were washed 3 times in 0.1 M PBS for 10 min each, and then incubated in a blocking solution containing 10% BSA in 0.1 M PBS with 0.5% Triton X-100 for 1 hr at RT. Slices were then incubated with primary antibodies (anti-TH) diluted in a solution containing 2% BSA in 0.1 M PBS with 0.1% Triton X-100 overnight at 4 °C. After washing with 0.1 M PBS 3 times, slices were incubated with the fluorophoreconjugated streptavidin (1:1000; Invitrogen) and Alexa Fluor-conjugated secondary antibodies (1:1000; Invitrogen) for 2 h. After washing with PBS 3 times, slices were mounted on microscope slides in an aqueous mounting medium (Aqua-Poly/Mount, Polysciences). Images were obtained with Zeiss LSM900 confocal microscope.

**RNAscope In situ hybridization—**Fixed brains were embedded in OCT (Tissue-Tek) and sectioned at a thickness of 12 μm. RNAscope Multiplex Fluorescent Reagent Kit v2 (ACD, Advanced Cell Diagnostics) was used following the manufacturer's manual for the fixed frozen tissues. Probe targeting *Swell1* (#458371) was purchased from ACD. TSA Plus fluorescein (#NEL741E001KT), Cyanine 3 (#NEL744001KT), or Cyanine 5 (#NEL745001KT) were used for developing the fluorescence signal. Images were collected with a 63x Plan Apochromat 1.40 NA oil immersion objective lens on a Zeiss LSM 900 confocal microscope and analyzed using ImageJ software.

## Electrophysiology

**Sniffer patch recording:** Sniffer patch recordings were performed as previously described [43]. Primary cultured astrocytes were used as the source cells, and HEK293T cells co-transfected with the α6, β3, and δ subunits of the $GABA_A$Rs were the sensor cells. 12–18 h after transfection, HEK293T cells were reseeded onto source cells for recording. To activate VRAC in astrocytes, recording electrodes (2–4 MΩ) were filled with a hypertonic internal solution containing (mM): 133 CsCl, 10 HEPES, 4 Mg-ATP, 0.5 $Na_3$-GTP, 2 $CaCl_2$, 5 EGTA, 100 mannitol, and 5 GABA (pH adjusted to 7.2 with CsOH and osmolality was 400–410 mOsm/kg). For HEK293T cells recording, the same internal solution was used except there was no mannitol and GABA. The external solution contained (in mM): 145 NaCl, 10 HEPES, 2 KCl, 2 $CaCl_2$, 1 $MgCl_2$, and 10 glucose (pH adjusted to pH 7.3 with NaOH and osmolality adjusted to 300–310 mOsm/kg). All the cells were held at −70 mV using Multiclamp 700B amplifier, and data were acquired with pClamp 10.7 software (Molecular Devices).

**Brain slice electrophysiology:** Mice were anesthetized with the inhalation anesthetic isoflurane and then perfused with ice-cold oxygenated cutting solution. The brain was removed rapidly and immersed in ice-cold choline-based cutting solution containing (in mM): 110 choline chloride, 7 $MgCl_2$, 2.5 KCl, 0.5 $CaCl_2$, 1.3 $NaH_2PO_4$, 25 $NaHCO_3$, 20 glucose, 3 kynurenic acids, saturated with 95% $O_2$ and 5% $CO_2$. Coronal slices of the VTA (250 μm) were cut in the cutting solution using a vibratome (VT-1200S, Leica) and transferred to artificial cerebrospinal fluid (aCSF) containing (in mM): 125 NaCl, 2.5 KCl, 2.5 $CaCl_2$, 1.3 $MgCl_2$, 1.3 $NaH_2PO_4$, 26 $NaHCO_3$, 10 glucose, saturated with 95% $O_2$ and 5% $CO_2$. The slices were allowed to recover for 30 min at 34 °C and then at RT for at least 1 h before recording. All recordings were made at RT in a submerged recording chamber with constant aCSF perfusion. Whole-cell recordings from VTA neurons were visualized under an upright microscope (BX51WI, Olympus) with infrared-differential interference contrast video microscopy and epifluorescence (Olympus). Recording pipettes were pulled by a micropipette puller (P1000, Sutter instrument) and had a resistance of 3–5 MΩ when filled with internal solutions. Recordings were made with MultiClamp 700B amplifier and 1550B digitizer (Molecular Device). Data acquisitions were performed with pClamp 10.7 software (Molecular Device), filtered at 1 kHz and digitized at 10 kHz. In all experiments, the series resistance (Rs) was monitored throughout the recording and controlled below 20 MΩ with no compensation. Data were discarded when the series resistance varied by ≥ 20%.

For tonic GABA current recordings, patch pipettes were filled with an internal solution containing (in mM): 135 KCl, 10 HEPES, 2 EGTA, 0.3 $Na_3$-ATP, 4 Mg-ATP, 0.5 $CaCl_2$, 10 phosphocreatine (pH 7.2, osmolality 280–290 mOsm/kg). Recording was performed in the presence of TTX (1 μM, Hello Bio) and glutamate receptors blockers (20 μM DNQX and 50 μM D-AP5, Hello Bio). Cells were held at −70 mV and the amplitude of tonic GABA current was measured by the baseline shift after bicuculine (100 μM, Tocris Bioscience) application. THIP-induced currents were measured by the baseline shift after THIP (Sigma) application, after that bicuculine was applied to verify the current was meditated by $GABA_A$Rs. For tonic NMDAR-mediated currents recording, neurons were held at +40 mV in normal aCSF with an internal solution containing (in mM): 110 Cs methylsulfate, 20 TEA-Cl, 15 CsCl, 4 ATP-Mg, 0.3 $Na_3$-GTP, 0.5 EGTA, 10 HEPES, 4.0 QX-314, and 1.0 spermine, pH adjusted to 7.2 with CsOH, osmolality 290–300 mOsm/kg with sucrose. Recording was performed in the presence of 1 μM TTX, 100 μM picrotoxin, and 20 μM DNQX. After the baseline was stable, tonic NMDAR current was observed by bath applying 100 μM D-AP5. Biocytin (1 mg/ml, Hello Bio) was added to the pipette solution for some recordings.

For cell-attached recordings, patch pipettes were filled with an internal solution containing (in mM): 125 K-gluconate, 15 KCl, 10 HEPES, 1 $MgCl_2$, 4 Mg-ATP, 0.3 $Na_3$-GTP, 10 phosphocreatine, and 0.2 EGTA (pH 7.2, osmolality 290–300 mOsm/kg). The firing rates were recorded for 5 min after basal firing was stable. For Fig. 4D, E, the firing rate was recorded for 3 min before and after THIP application.

## Behavioral assays

**Locomotor sensitization:** Mice were handled by investigators for five days before the behavioral test. After saline or cocaine (Sigma) i.p. injection (15 mg/kg), mice were immediately placed in a standard cage inside infrared locomotion chambers (18' × 18') (Photobeam activity system-San Diego Instruments) and monitored for movement by using horizontal photobeams. Beam breaks were converted to directionally specific movements and summated at 5-min intervals over 1 hr. Ambulatory activity (beam breaks) was measured as total horizontal photobeam breaks.

**Conditioned place preference:** Mice were handled by investigators for five days before the test. The conditioned place preference was performed in spatial place preference boxes (LE895, Harvard Apparatus) and consisted of three sessions over 8 d. A video tracking system (ANY-maze, Stoelting) recorded all animal movements. We used an unbiased, counterbalanced protocol. On day 1, individual mice were placed in the neutral (middle) compartment and allowed to freely explore the entire apparatus for 15 min (pre-test). On days 2–7 (training session), mice were trained for 6 consecutive days with alternating injections of cocaine (10 mg/kg, i.p.) or saline in the designated compartments. On days 2, 4, and 6, mice received cocaine injections and were immediately confined to one side of the chambers (conditioned compartment) for 30 min. On days 3, 5, and 7, mice received saline injections and were immediately confined to the opposite chamber (unconditioned compartment) for 30 min. Mice were returned to their home cages after each training. On day 8, like day 1, mice were placed in the middle compartment and allowed to explore the entire apparatus for 15 min (posttest). CPP scores were defined as the time (s) spent in drug paired compartment minus time (s) spent in saline paired compartment pre- and post-conditioning.

**Quantification and statistical analysis—**GraphPad Prism 8.3.0 software was used for all statistical analyses. Images were analyzed with ImageJ (US National Institutes of Health) and ZEN software (ZEISS). Before each test, normality distribution of the data was assessed using Shapiro-Wilk normality test. Parametric tests (paired or unpaired Student's t test for two groups) were used for normally distributed data while non-parametric tests (Mann-Whitney for unpaired two groups) were used for data not normally distributed. One-way ANOVA followed by Tukey's post hoc test were used for statistical analyses with more than three samples. Two-way ANOVA followed by Bonferroni's post hoc test was used to analyze studies that have two factors. Data are reported as mean ± SEM. The significance level was set at $p < 0.05$. n numbers, test statistics, and exact *p* values are indicated in the figure legends. No statistical methods were used to predetermine sample sizes, but our sample sizes are similar to those reported in previous publications [16,43]. For behaviors, animals with missed viral injections or significant viral spread outside the targeted region were excluded from analyses. All behavioral assays were repeated in at least three cohorts of animals. The other experiments were pooled from at least three individual animals and collected from at least two rounds of experiments. Experimental and control animals were randomized throughout the study. Investigators were blinded to allocation of groups and outcome assessment for all experiments except for Figs. 2J, K, 5B, and Figs. S1, 2, 4,

7 in which the experimental conditions were obvious to the researchers or there were no comparisons.

## Supplementary Material

Refer to Web version on PubMed Central for supplementary material.

## Acknowledgements

We thank Jamie Maguire for providing the *Gabrd* KO mice, George Richerson for $GABA_A$ receptors plasmids, and Hiroshi Yamaguchi for pAAV-CAG-DIO-mCherry constructs. We thank members of the Qiu lab for valuable discussion. J.Y. is supported by an AHA and American Brain Foundation postdoctoral fellowship (20POST35200185), an AHA Career Development Award (857671), and a NARSAD Young Investigator Grant (30235). J.C. is supported by an AHA postdoctoral fellowship (19POST34410020). J.B. is supported by the NIH grant (P50DA044123). Z.Q. is supported by a McKnight Scholar award, a Klingenstein-Simon Scholar award, a Sloan Research Fellowship in Neuroscience, and the NIH grants (R35GM124824 and R01NS118014).

### Inclusion and diversity

We support inclusive, diverse, and equitable conduct of research.

## Data and materials availability

All data are available in the main text or the supplementary material.

## References

1. Koob GF, and Bloom FE (1988). Cellular and molecular mechanisms of drug dependence. Science 242, 715–723. 10.1126/science.2903550. [PubMed: 2903550]
2. Nestler EJ (2005). Is there a common molecular pathway for addiction? Nat Neurosci 8, 1445–1449. 10.1038/nn1578. [PubMed: 16251986]
3. Ungless MA, Whistler JL, Malenka RC, and Bonci A. (2001). Single cocaine exposure in vivo induces long-term potentiation in dopamine neurons. Nature 411, 583–587. 10.1038/35079077. [PubMed: 11385572]
4. Saal D, Dong Y, Bonci A, and Malenka RC (2003). Drugs of abuse and stress trigger a common synaptic adaptation in dopamine neurons. Neuron 37, 577–582. 10.1016/s08966273(03)00021-7. [PubMed: 12597856]
5. Johnson SW, and North RA (1992). Opioids excite dopamine neurons by hyperpolarization of local interneurons. J Neurosci 12, 483–488. [PubMed: 1346804]
6. Bocklisch C, Pascoli V, Wong JC, House DR, Yvon C, de Roo M, Tan KR, and Luscher C. (2013). Cocaine disinhibits dopamine neurons by potentiation of GABA transmission in the ventral tegmental area. Science 341, 1521–1525. 10.1126/science.1237059. [PubMed: 24072923]
7. Tan KR, Brown M, Labouebe G, Yvon C, Creton C, Fritschy JM, Rudolph U, and Luscher C. (2010). Neural bases for addictive properties of benzodiazepines. Nature 463, 769–774. 10.1038/nature08758. [PubMed: 20148031]
8. Steffensen SC., Taylor SR., Horton ML., Barber EN., Lyl LT., Stobbs SH., and Allison DW. (2008). Cocaine disinhibits dopamine neurons in the ventral tegmental area via use-dependent blockade of GABA neuron voltage-sensitive sodium channels. Eur J Neurosci 28, 2028–2040. 10.1111/j.1460-9568.2008.06479.x. [PubMed: 19046384]
9. Johnson SW, and North RA (1992). Two types of neurone in the rat ventral tegmental area and their synaptic inputs. J Physiol 450, 455–468. 10.1113/jphysiol.1992.sp019136. [PubMed: 1331427]
10. Morales M, and Margolis EB (2017). Ventral tegmental area: cellular heterogeneity, connectivity and behaviour. Nat Rev Neurosci 18, 73–85. 10.1038/nrn.2016.165. [PubMed: 28053327]

11. Farrant M, and Nusser Z. (2005). Variations on an inhibitory theme: phasic and tonic activation of GABA(A) receptors. Nat Rev Neurosci 6, 215–229. 10.1038/nrn1625. [PubMed: 15738957]
12. Belelli D, Harrison NL, Maguire J, Macdonald RL, Walker MC, and Cope DW (2009). Extrasynaptic GABAA receptors: form, pharmacology, and function. J Neurosci 29, 12757–12763. 10.1523/JNEUROSCI.3340-09.2009. [PubMed: 19828786]
13. Lee V, and Maguire J. (2014). The impact of tonic GABAA receptor-mediated inhibition on neuronal excitability varies across brain region and cell type. Front Neural Circuits 8, 3. 10.3389/fncir.2014.00003. [PubMed: 24550784]
14. Brickley SG, and Mody I. (2012). Extrasynaptic GABA(A) receptors: their function in the CNS and implications for disease. Neuron 73, 23–34. 10.1016/j.neuron.2011.12.012. [PubMed: 22243744]
15. Lee S, Yoon BE, Berglund K, Oh SJ, Park H, Shin HS, Augustine GJ, and Lee CJ (2010). Channel-mediated tonic GABA release from glia. Science 330, 790–796. 10.1126/science.1184334. [PubMed: 20929730]
16. Qiu Z, Dubin AE, Mathur J, Tu B, Reddy K, Miraglia LJ, Reinhardt J, Orth AP, and Patapoutian A. (2014). SWELL1, a plasma membrane protein, is an essential component of volume-regulated anion channel. Cell 157, 447–458. 10.1016/j.cell.2014.03.024. [PubMed: 24725410]
17. Voss FK, Ullrich F, Munch J, Lazarow K, Lutter D, Mah N, Andrade-Navarro MA, von Kries JP, Stauber T, and Jentsch TJ (2014). Identification of LRRC8 heteromers as an essential component of the volume-regulated anion channel VRAC. Science 344, 634–638. 10.1126/science.1252826. [PubMed: 24790029]
18. Osei-Owusu J, Yang J, Vitery MDC, and Qiu Z. (2018). Molecular Biology and Physiology of Volume-Regulated Anion Channel (VRAC). Curr Top Membr 81, 177–203. 10.1016/bs.ctm.2018.07.005. [PubMed: 30243432]
19. Lutter D, Ullrich F, Lueck JC, Kempa S, and Jentsch TJ (2017). Selective transport of neurotransmitters and modulators by distinct volume-regulated LRRC8 anion channels. J Cell Sci 130, 1122–1133. 10.1242/jcs.196253. [PubMed: 28193731]
20. Menegaz D, Hagan DW, Almaca J, Cianciaruso C, Rodriguez-Diaz R, Molina J, Dolan RM, Becker MW, Schwalie PC, Nano R, et al. (2019). Mechanism and effects of pulsatile GABA secretion from cytosolic pools in the human beta cell. Nat Metab 1, 1110–1126. 10.1038/s42255-019-0135-7. [PubMed: 32432213]
21. Vashchinkina E, Manner AK, Vekovischeva O, den Hollander B, Uusi-Oukari M, Aitta-Aho T, and Korpi ER (2014). Neurosteroid Agonist at GABAA receptor induces persistent neuroplasticity in VTA dopamine neurons. Neuropsychopharmacology 39, 727–737. 10.1038/npp.2013.258. [PubMed: 24077066]
22. Peron SP, Freeman J, Iyer V, Guo C, and Svoboda K. (2015). A Cellular Resolution Map of Barrel Cortex Activity during Tactile Behavior. Neuron 86, 783–799. 10.1016/j.neuron.2015.03.027. [PubMed: 25913859]
23. Corr J., van Zesse R., Loureir M., Patriarch T., Tia L., Pascol V., and Lusche C. (2018). Dopamine neurons projecting to medial shell of the nucleus accumbens drive heroin reinforcement. Elife 7. 10.7554/eLife.39945.
24. Ito R, Robbins TW, and Everitt BJ (2004). Differential control over cocaine-seeking behavior by nucleus accumbens core and shell. Nat Neurosci 7, 389–397. 10.1038/nn1217. [PubMed: 15034590]
25. Fuchs RA, Ramirez DR, and Bell GH (2008). Nucleus accumbens shell and core involvement in drug context-induced reinstatement of cocaine seeking in rats. Psychopharmacology (Berl) 200, 545–556. 10.1007/s00213-008-1234-4. [PubMed: 18597075]
26. Lammel S, Hetzel A, Hackel O, Jones I, Liss B, and Roeper J. (2008). Unique properties of mesoprefrontal neurons within a dual mesocorticolimbic dopamine system. Neuron 57, 760–773. 10.1016/j.neuron.2008.01.022. [PubMed: 18341995]
27. Yang H, de Jong JW, Tak Y, Peck J, Bateup HS, and Lammel S. (2018). Nucleus Accumbens Subnuclei Regulate Motivated Behavior via Direct Inhibition and Disinhibition of VTA Dopamine Subpopulations. Neuron 97, 434–449 e434. 10.1016/j.neuron.2017.12.022. [PubMed: 29307710]

28. Pirker S, Schwarzer C, Wieselthaler A, Sieghart W, and Sperk G. (2000). GABA(A) receptors: immunocytochemical distribution of 13 subunits in the adult rat brain. Neuroscience 101, 815850. 10.1016/s0306-4522(00)00442-5.
29. Hortnagl H, Tasan RO, Wieselthaler A, Kirchmair E, Sieghart W, and Sperk G. (2013). Patterns of mRNA and protein expression for 12 GABAA receptor subunits in the mouse brain. Neuroscience 236, 345–372. 10.1016/j.neuroscience.2013.01.008. [PubMed: 23337532]
30. Mihalek RM, Banerjee PK, Korpi ER, Quinlan JJ, Firestone LL, Mi ZP, Lagenaur C, Tretter V, Sieghart W, Anagnostaras SG, et al. (1999). Attenuated sensitivity to neuroactive steroids in gamma-aminobutyrate type A receptor delta subunit knockout mice. Proc Natl Acad Sci U S A 96, 12905–12910. 10.1073/pnas.96.22.12905. [PubMed: 10536021]
31. Kwak H, Koh W, Kim S, Song K, Shin JI, Lee JM, Lee EH, Bae JY, Ha GE, Oh JE, et al. (2020). Astrocytes Control Sensory Acuity via Tonic Inhibition in the Thalamus. Neuron 108, 691–706 e610. 10.1016/j.neuron.2020.08.013. [PubMed: 32905785]
32. Sun H, Tsunenari T, Yau KW, and Nathans J. (2002). The vitelliform macular dystrophy protein defines a new family of chloride channels. Proc Natl Acad Sci U S A 99, 4008–4013. 10.1073/pnas.052692999. [PubMed: 11904445]
33. Kane Dickson V, Pedi L, and Long SB (2014). Structure and insights into the function of a Ca(2+)-activated Cl(−) channel. Nature 516, 213–218. 10.1038/nature13913. [PubMed: 25337878]
34. Vaisey G, Miller AN, and Long SB (2016). Distinct regions that control ion selectivity and calcium-dependent activation in the bestrophin ion channel. Proc Natl Acad Sci U S A 113, E7399–E7408. 10.1073/pnas.1614688113. [PubMed: 27821745]
35. Saunders A, Macosko EZ, Wysoker A, Goldman M, Krienen FM, de Rivera H, Bien E, Baum M, Bortolin L, Wang S, et al. (2018). Molecular Diversity and Specializations among the Cells of the Adult Mouse Brain. Cell 174, 1015–1030 e1016. 10.1016/j.cell.2018.07.028. [PubMed: 30096299]
36. Bianchi MT, Haas KF, and Macdonald RL (2002). Alpha1 and alpha6 subunits specify distinct desensitization, deactivation and neurosteroid modulation of GABA(A) receptors containing the delta subunit. Neuropharmacology 43, 492–502. 10.1016/s0028-3908(02)00163-6. [PubMed: 12367596]
37. Tao J, Wu H, Lin Q, Wei W, Lu XH, Cantle JP, Ao Y, Olsen RW, Yang XW, Mody I, et al. (2011). Deletion of astroglial Dicer causes non-cell-autonomous neuronal dysfunction and degeneration. J Neurosci 31, 8306–8319. 10.1523/JNEUROSCI.0567-11.2011. [PubMed: 21632951]
38. Nestler EJ, and Luscher C. (2019). The Molecular Basis of Drug Addiction: Linking Epigenetic to Synaptic and Circuit Mechanisms. Neuron 102, 48–59. 10.1016/j.neuron.2019.01.016. [PubMed: 30946825]
39. Liu QS, Pu L, and Poo MM (2005). Repeated cocaine exposure in vivo facilitates LTP induction in midbrain dopamine neurons. Nature 437, 1027–1031. 10.1038/nature04050. [PubMed: 16222299]
40. Luscher C, and Malenka RC (2011). Drug-evoked synaptic plasticity in addiction: from molecular changes to circuit remodeling. Neuron 69, 650–663. 10.1016/j.neuron.2011.01.017. [PubMed: 21338877]
41. Lewitus GM, Konefal SC, Greenhalgh AD, Pribiag H, Augereau K, and Stellwagen D. (2016). Microglial TNF-alpha Suppresses Cocaine-Induced Plasticity and Behavioral Sensitization. Neuron 90, 483–491. 10.1016/j.neuron.2016.03.030. [PubMed: 27112496]
42. Sah P, Hestrin S, and Nicoll RA (1989). Tonic activation of NMDA receptors by ambient glutamate enhances excitability of neurons. Science 246, 815–818. 10.1126/science.2573153. [PubMed: 2573153]
43. Yan J., Viter MDC., Che J., Osei-Owus J., Ch J., and Qi Z. (2019). Glutamate-Releasing SWELL1 Channel in Astrocytes Modulates Synaptic Transmission and Promotes Brain Damage in Stroke. Neuron 102, 813–827 e816. 10.1016/j.neuron.2019.03.029. [PubMed: 30982627]
44. Yu X, Taylor AMW, Nagai J, Golshani P, Evans CJ, Coppola G, and Khakh BS (2018). Reducing Astrocyte Calcium Signaling In Vivo Alters Striatal Microcircuits and Causes Repetitive Behavior. Neuron 99, 1170–1187 e1179. 10.1016/j.neuron.2018.08.015. [PubMed: 30174118]
45. Wu Z, Guo Z, Gearing M, and Chen G. (2014). Tonic inhibition in dentate gyrus impairs long-term potentiation and memory in an Alzheimer's [corrected] disease model. Nat Commun 5, 4159. 10.1038/ncomms5159. [PubMed: 24923909]

46. Jo S, Yarishkin O, Hwang YJ, Chun YE, Park M, Woo DH, Bae JY, Kim T, Lee J, Chun H, et al. (2014). GABA from reactive astrocytes impairs memory in mouse models of Alzheimer's disease. Nat Med 20, 886–896. 10.1038/nm.3639. [PubMed: 24973918]
47. Clarkson AN, Huang BS, Macisaac SE, Mody I, and Carmichael ST (2010). Reducing excessive GABA-mediated tonic inhibition promotes functional recovery after stroke. Nature 468, 305–309. 10.1038/nature09511. [PubMed: 21048709]
48. Escartin C, Galea E, Lakatos A, O'Callaghan JP, Petzold GC, Serrano-Pozo A, Steinhauser C, Volterra A, Carmignoto G, Agarwal A, et al. (2021). Reactive astrocyte nomenclature, definitions, and future directions. Nat Neurosci 24, 312–325. 10.1038/s41593-020-00783-4. [PubMed: 33589835]
49. Vanderschuren LJ, and Kalivas PW (2000). Alterations in dopaminergic and glutamatergic transmission in the induction and expression of behavioral sensitization: a critical review of preclinical studies. Psychopharmacology (Berl) 151, 99–120. 10.1007/s002130000493. [PubMed: 10972458]
50. Bardo MT, and Bevins RA (2000). Conditioned place preference: what does it add to our preclinical understanding of drug reward? Psychopharmacology (Berl) 153, 31–43. 10.1007/s002130000569. [PubMed: 11255927]
51. Yamaguchi H, Hopf FW, Li SB, and de Lecea L. (2018). In vivo cell type-specific CRISPR knockdown of dopamine beta hydroxylase reduces locus coeruleus evoked wakefulness. Nat Commun 9, 5211. 10.1038/s41467-018-07566-3. [PubMed: 30523254]
52. Platt RJ, Chen S, Zhou Y, Yim MJ, Swiech L, Kempton HR, Dahlman JE, Parnas O, Eisenhaure TM, Jovanovic M, et al. (2014). CRISPR-Cas9 knockin mice for genome editing and cancer modeling. Cell 159, 440–455. 10.1016/j.cell.2014.09.014. [PubMed: 25263330]
53. Jhou TC, Fields HL, Baxter MG, Saper CB, and Holland PC (2009). The rostromedial tegmental nucleus (RMTg), a GABAergic afferent to midbrain dopamine neurons, encodes aversive stimuli and inhibits motor responses. Neuron 61, 786–800. 10.1016/j.neuron.2009.02.001. [PubMed: 19285474]
54. Sode ME., Chun AS., Cueva B., Resnic JM., Awatraman R., and Zweife LS. (2020). Anatomic resolution of neurotransmitter-specific projections to the VTA reveals diversity of GABAergic inputs. Nat Neurosci 23, 968–980. 10.1038/s41593-020-0657-z. [PubMed: 32541962]
55. Szabo B, Siemes S, and Wallmichrath I. (2002). Inhibition of GABAergic neurotransmission in the ventral tegmental area by cannabinoids. Eur J Neurosci 15, 2057–2061. 10.1046/j.14609568.2002.02041.x. [PubMed: 12099913]
56. Cruz HG, Ivanova T, Lunn ML, Stoffel M, Slesinger PA, and Luscher C. (2004). Bidirectional effects of GABA(B) receptor agonists on the mesolimbic dopamine system. Nat Neurosci 7, 153–159. 10.1038/nn1181. [PubMed: 14745451]
57. Mansvelder HD, Keath JR, and McGehee DS (2002). Synaptic mechanisms underlie nicotine-induced excitability of brain reward areas. Neuron 33, 905–919. 10.1016/s08966273(02)00625-6. [PubMed: 11906697]
58. Oberheim NA, Goldman SA, and Nedergaard M. (2012). Heterogeneity of astrocytic form and function. Methods Mol Biol 814, 23–45. 10.1007/978-1-61779-452-0_3. [PubMed: 22144298]
59. Khakh BS, and Deneen B. (2019). The Emerging Nature of Astrocyte Diversity. Annu Rev Neurosci 42, 187–207. 10.1146/annurev-neuro-070918-050443. [PubMed: 31283899]
60. Khakh BS, and Sofroniew MV (2015). Diversity of astrocyte functions and phenotypes in neural circuits. Nat Neurosci 18, 942–952. 10.1038/nn.4043. [PubMed: 26108722]
61. Ben Haim L, and Rowitch DH (2017). Functional diversity of astrocytes in neural circuit regulation. Nat Rev Neurosci 18, 31–41. 10.1038/nrn.2016.159. [PubMed: 27904142]
62. Syeda R, Qiu Z, Dubin AE, Murthy SE, Florendo MN, Mason DE, Mathur J, Cahalan SM, Peters EC, Montal M, and Patapoutian A. (2016). LRRC8 Proteins Form Volume-Regulated Anion Channels that Sense Ionic Strength. Cell 164, 499–511. 10.1016/j.cell.2015.12.031. [PubMed: 26824658]
63. Martin R, Bajo-Graneras R, Moratalla R, Perea G, and Araque A. (2015). Circuit-specific signaling in astrocyte-neuron networks in basal ganglia pathways. Science 349, 730–734. 10.1126/science.aaa7945. [PubMed: 26273054]

64. Gomez JA, Perkins JM, Beaudoin GM, Cook NB, Quraishi SA, Szoeke EA, Thangamani K, Tschumi CW, Wanat MJ, Maroof AM, et al. (2019). Ventral tegmental area astrocytes orchestrate avoidance and approach behavior. Nat Commun 10, 1455. 10.1038/s41467-01909131-y. [PubMed: 30926783]

65. Zhou JJ, Luo Y, Chen SR, Shao JY, Sah R, and Pan HL (2020). LRRC8A-dependent volume-regulated anion channels contribute to ischemia-induced brain injury and glutamatergic input to hippocampal neurons. Exp Neurol 332, 113391. 10.1016/j.expneurol.2020.113391.

66. Takumi T, Ishii T, Horio Y, Morishige K, Takahashi N, Yamada M, Yamashita T, Kiyama H, Sohmiya K, Nakanishi S, and et al. (1995). A novel ATP-dependent inward rectifier potassium channel expressed predominantly in glial cells. J Biol Chem 270, 16339–16346. 10.1074/jbc.270.27.16339. [PubMed: 7608203]

67. Nagai J, Rajbhandari AK, Gangwani MR, Hachisuka A, Coppola G, Masmanidis SC, Fanselow MS, and Khakh BS (2019). Hyperactivity with Disrupted Attention by Activation of an Astrocyte Synaptogenic Cue. Cell 177, 1280–1292 e1220. 10.1016/j.cell.2019.03.019. [PubMed: 31031006]

68. Kruyer A, and Kalivas PW (2021). Astrocytes as cellular mediators of cue reactivity in addiction. Curr Opin Pharmacol 56, 1–6. 10.1016/j.coph.2020.07.009. [PubMed: 32862045]

69. Reissner KJ, and Pletnikov MV (2020). Contributions of nonneuronal brain cells in substance use disorders. Neuropsychopharmacology 45, 224–225. 10.1038/s41386-019-0494-5. [PubMed: 31477816]

70. Wang J, Li KL, Shukla A, Beroun A, Ishikawa M, Huang X, Wang Y, Wang YQ, Yang Y, Bastola ND, et al. (2021). Cocaine Triggers Astrocyte-Mediated Synaptogenesis. Biol Psychiatry 89, 386–397. 10.1016/j.biopsych.2020.08.012. [PubMed: 33069367]

71. Shelkar GP, Gandhi PJ, Liu J, and Dravid SM (2022). Cocaine preference and neuroadaptations are maintained by astrocytic NMDA receptors in the nucleus accumbens. Sci Adv 8, eabo6574. 10.1126/sciadv.abo6574.

72. Bowers MS, and Kalivas PW (2003). Forebrain astroglial plasticity is induced following withdrawal from repeated cocaine administration. Eur J Neurosci 17, 1273–1278. 10.1046/j.1460-9568.2003.02537.x. [PubMed: 12670315]

73. Beitner-Johnso D., Guitar X., and Nestle EJ. (1993). Glial fibrillary acidic protein and the mesolimbic dopamine system: regulation by chronic morphine and Lewis-Fischer strain differences in the rat ventral tegmental area. J Neurochem 61, 1766–1773. 10.1111/j.1471-4159.1993.tb09814.x. [PubMed: 8228992]

74. Kim R, Sepulveda-Orengo MT, Healey KL, Williams EA, and Reissner KJ (2018). Regulation of glutamate transporter 1 (GLT-1) gene expression by cocaine self-administration and withdrawal. Neuropharmacology 128, 1–10. 10.1016/j.neuropharm.2017.09.019. [PubMed: 28919080]

75. Scofield MD, Li H, Siemsen BM, Healey KL, Tran PK, Woronoff N, Boger HA, Kalivas PW, and Reissner KJ (2016). Cocaine Self-Administration and Extinction Leads to Reduced Glial Fibrillary Acidic Protein Expression and Morphometric Features of Astrocytes in the Nucleus Accumbens Core. Biol Psychiatry 80, 207–215. 10.1016/j.biopsych.2015.12.022. [PubMed: 26946381]

76. Sharpe AL, Trzeciak M, Eliason NL, Blankenship HE, Byrd BAM, Douglas PD, Freeman WM, and Beckstead MJ (2022). Repeated cocaine or methamphetamine treatment alters astrocytic CRF2 and GLAST expression in the ventral midbrain. Addict Biol 27, e13120. 10.1111/adb.13120.

77. Corkrum M, Covelo A, Lines J, Bellocchio L, Pisansky M, Loke K, Quintana R, Rothwell PE, Lujan R, Marsicano G, et al. (2020). Dopamine-Evoked Synaptic Regulation in the Nucleus Accumbens Requires Astrocyte Activity. Neuron 105, 1036–1047 e1035. 10.1016/j.neuron.2019.12.026. [PubMed: 31954621]

## Highlights

- VTA astrocytes release GABA through Swell1 channels to mediate tonic inhibition
- Cocaine selectively potentiates tonic inhibition onto VTA GABA neurons in mice
- Astrocytic Swell1 channel contributes to cocaine-induced tonic inhibition
- Attenuation of tonic inhibition in VTA reduces cocaine reward behaviors

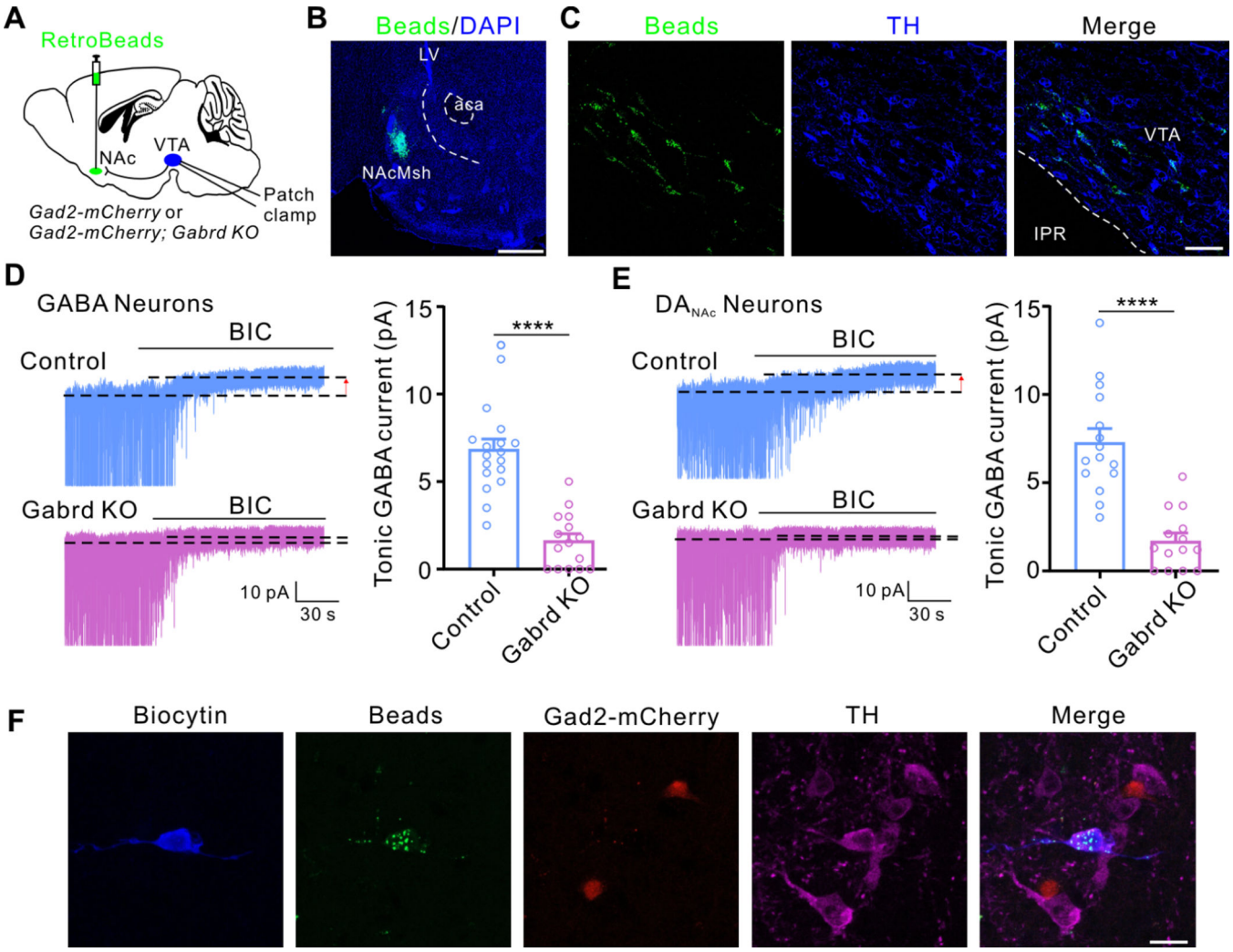


**Figure 1. δ-GABA$_A$Rs mediate tonic inhibition currents in VTA GABA and DA$_{NAc}$ neurons.**

**A**, Scheme of the specific labeling and whole-cell patch-clamp recordings of VTA GABA and NAc medial shell-projecting DA neurons (DA$_{NAc}$).

**B**, Representative image of the injection site with green beads located in the NAc medial shell (NAcMsh). LV, lateral ventricle; aca, anterior commissure. Scale bar, 500 μm.

**C**, Representative images of green bead-labeled TH-immunopositive DA neurons. IPR, interpeduncular nucleus. Scale bar, 50 μm.

**D**, **E**, Traces (left) and quantifications (right) of tonic inhibition current recordings from VTA GABA (**D**) and DA$_{NAc}$ neurons (**E**) in control and Gabrd KO mice. Dashed lines and arrows indicate the changes of baseline induced by bicuculline application (BIC; 100 μM). GABA neurons: n = 15–18 cells from 5 mice per genotype. DA$_{NAc}$ neurons: n = 14–15 cells from 5 mice per genotype.

**F**, Example confocal images showing a biocytin-filled (blue), retrogradely labeled (green), TH-immunopositive (magenta) cell in the Gad2-mCherry (red) mice. Scale bar, 20 μm.

Data are reported as mean ± SEM. Student's t tests for **D** and **E**, ****$p < 0.0001$.

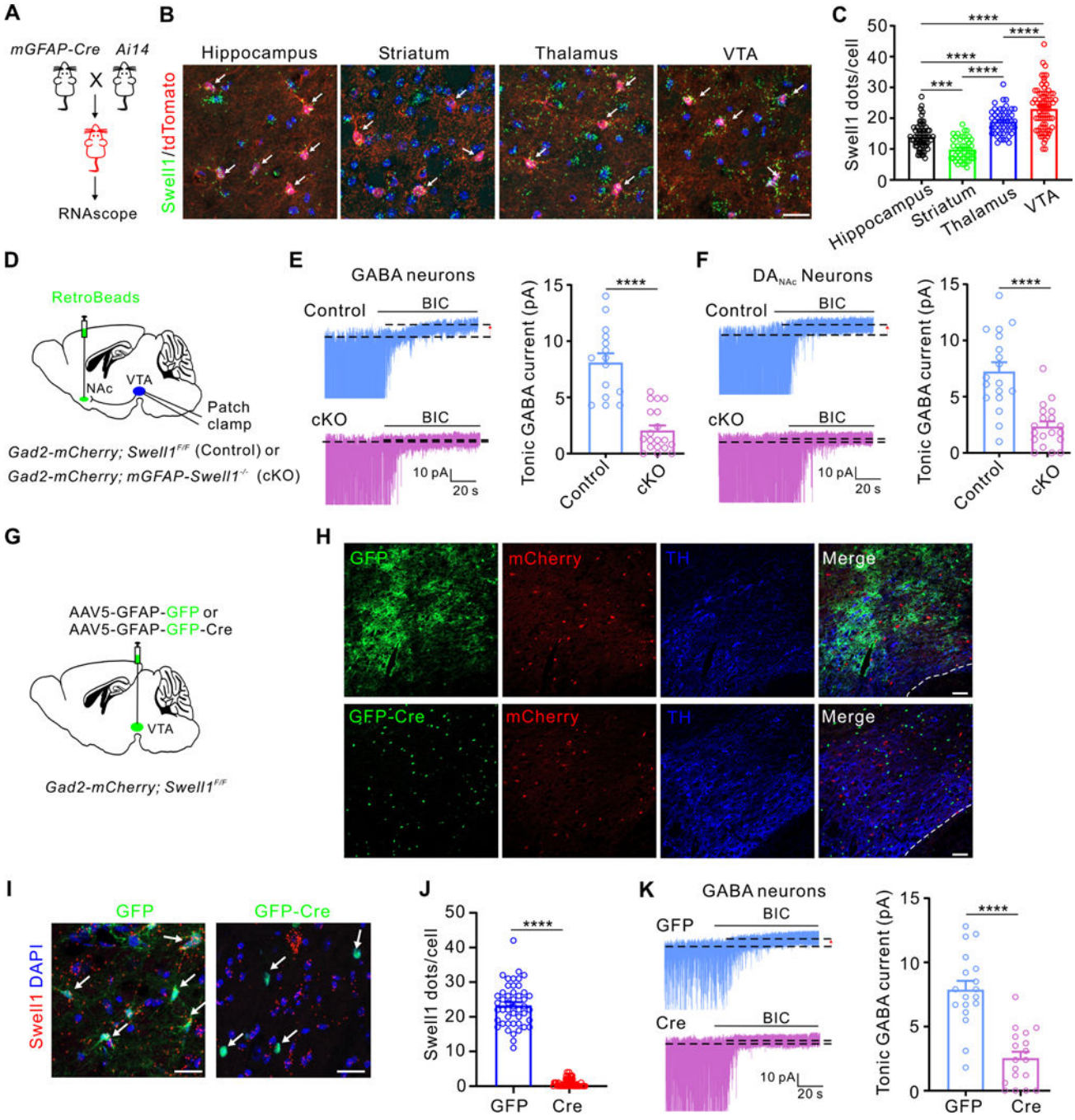


**Figure 2. GABA-permeable Swell1 channel in VTA astrocytes mediates tonic inhibition.**

**A**, Scheme of the experimental design.

**B**, Representative images of *Swell1* RNAscope in situ hybridization in different brain regions from GFAP-Ai14 mice where astrocytes were labeled with tdTomato (red). Scale bar, 20 μm.

**C**, Quantification of *Swell1* mRNA in situ hybridization signals. n = 45–77 cells from 3–4 mice per group.

**D**, Scheme of the specific labeling and whole-cell patch-clamp recordings of VTA GABA and $DA_{NAc}$ neurons in control and *Swell1* cKO mice.

**E** and **F**, Traces (left) and quantifications (right) of tonic inhibition current recordings from VTA GABA (**E**) and $DA_{NAc}$ neurons (**F**) in control and *Swell1* cKO mice. GABA neurons: n = 15–19 cells from 5–6 mice per genotype. $DA_{NAc}$ neurons: n = 18–19 cells from 6 mice per group.

**G**, Schematic showing AAV strategy used to delete *Swell1* selectively in VTA astrocytes.

**H**, Confocal images showing the expression of GFP and GFP-Cre in VTA astrocytes. GABA neurons were labeled with mCherry. DA neurons were immunostained with TH. Scale bar, 50 μm.

**I**, Representative images of *Swell1* RNAscope in situ hybridization in VTA from GFP- and Cre-expressing mice. Arrows indicate virus-infected astrocytes. Scale bar, 20 μm.

**J**, Quantification of *Swell1* mRNA in situ hybridization signals of GFP-positive cells. n = 47–48 cells from 3 mice per group.

**K**, Traces (left) and quantifications (right) of tonic inhibition current recordings from VTA GABA neurons of AAV injected mice. n = 18 cells from 5 mice per group.

Data are reported as mean ± SEM. One-way ANOVA, Tukey's post hoc test for **C**. Student's t tests for **E**, **F**, and **K**. Mann-Whitney test for **J**. ***p < 0.001, ****p < 0.0001.

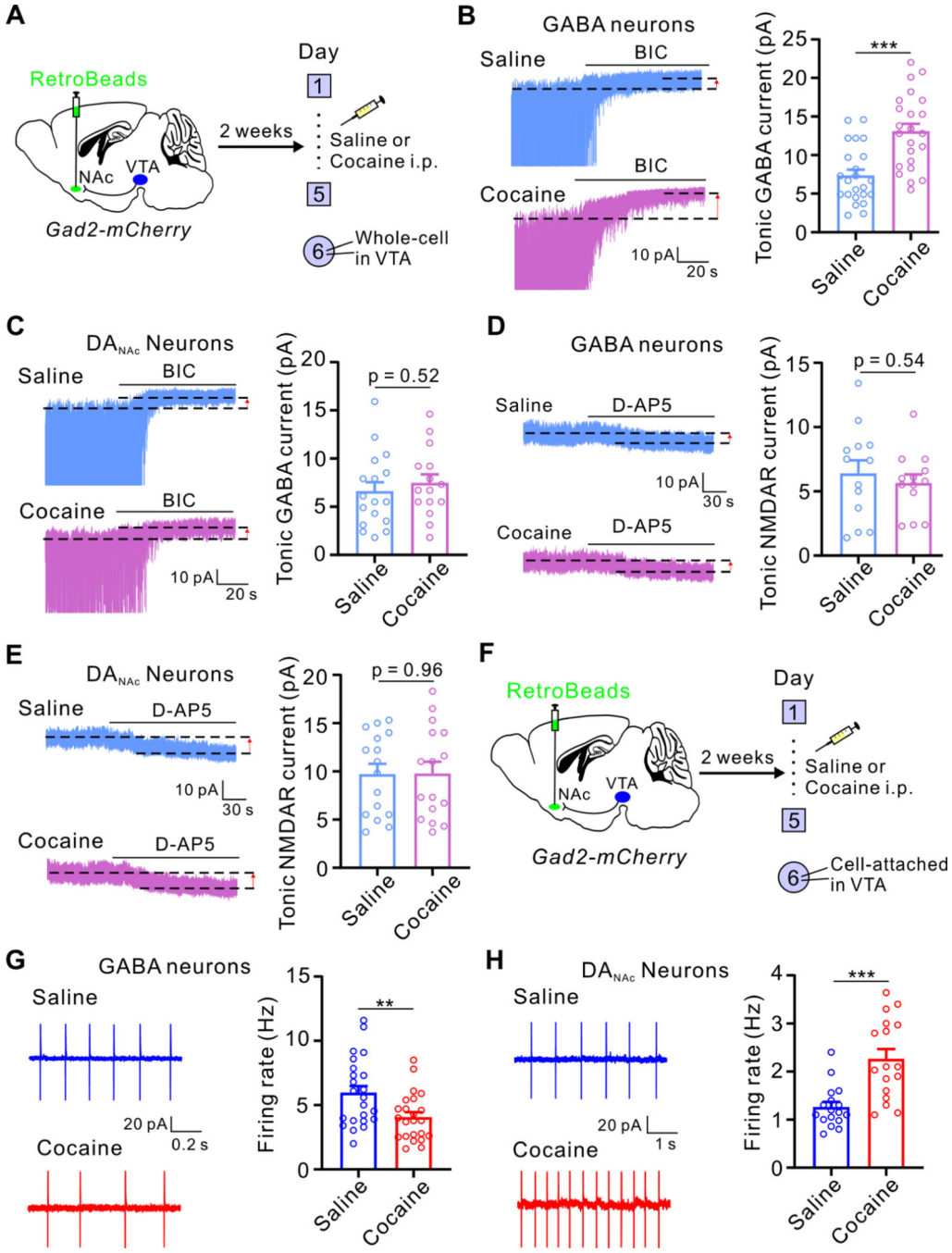


**Figure 3. Potentiation of tonic inhibition onto VTA GABA neurons by cocaine.**

**A**, Scheme of the experimental protocol.

**B-E**, Traces (left) and quantifications (right) of tonic inhibition (**B**, **C**) or tonic NMDAR (**D**, **E**) current recordings from VTA GABA (**B, D**) and DA$_{NAc}$ neurons (**C, E**) in saline or cocaine-injected Gad2-mCherry mice. Dashed lines and arrows indicate the changes of baseline induced by bicuculline (BIC; 100 μM) or D-AP5 (50 μM) application. Cells were held at +40 mV for (**D**), (**E**). GABA neurons: n = 23 cells from 6 mice per group for (**B**); n

= 13 cells from 4 mice per group for **(D)**. $DA_{NAc}$ neurons: n = 15–17 cells from 5 mice per group for (**C**); n = 16 cells from 4 mice per group for (**E**).

**F**, Scheme of the experimental protocol.

**G, H,** Traces (left) and quantifications (right) of cell-attached recordings from VTA GABA **(G)** and DANAc neurons **(H)** in saline or cocaine injected Gad2-mCherry mice. GABA neurons: n = 23 cells from 5 mice per group. $DA_{NAc}$ neurons: n = 17 cells from 5 mice per group.

Data are reported as mean ± SEM. Student's t tests for **B-E, G,** and **H.** **p < 0.01, ***p < 0.001.

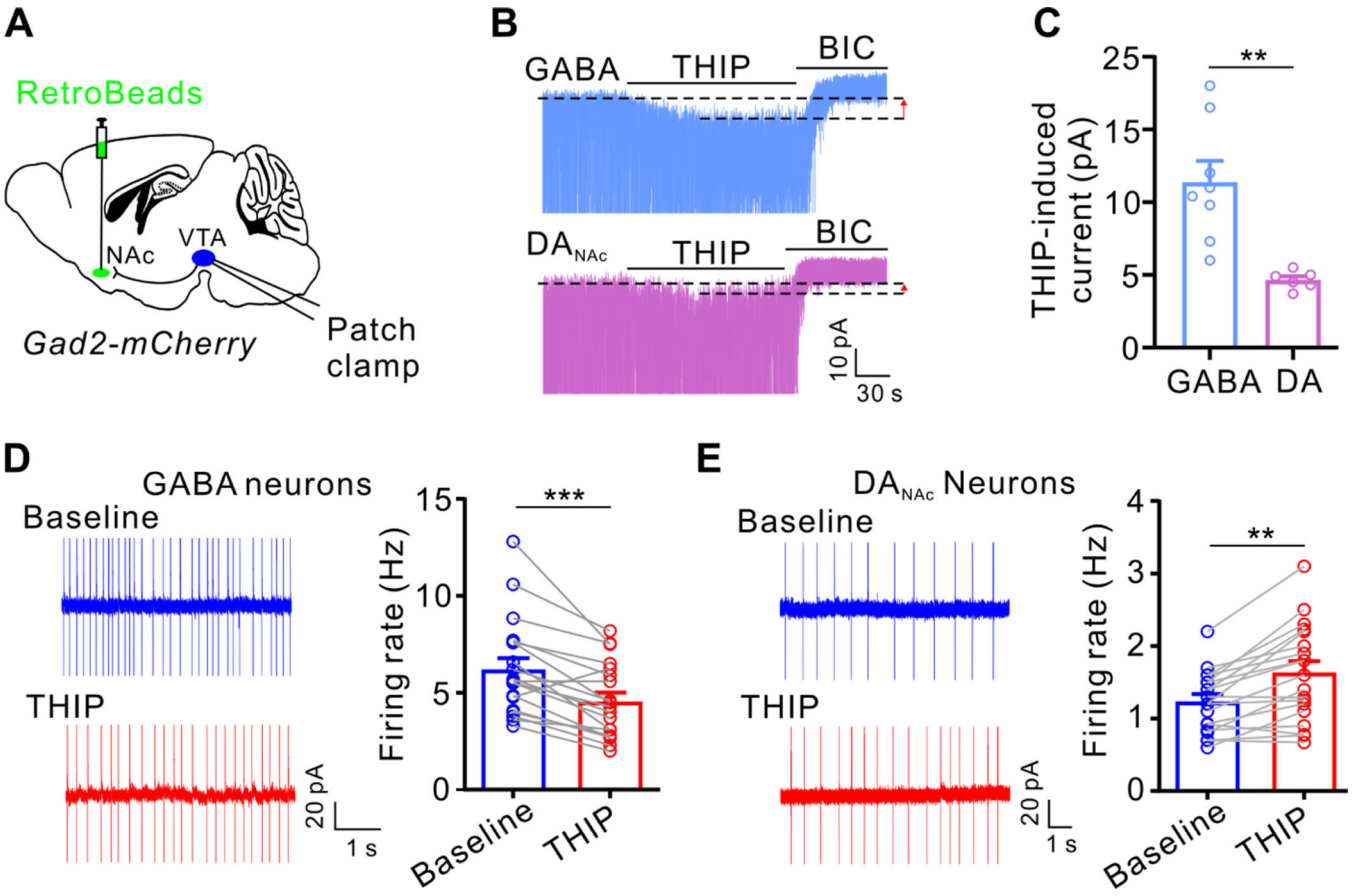


**Figure 4. Activation of δ-GABA$_A$Rs by THIP inhibits VTA GABA neurons, resulting in disinhibition of DA$_{NAc}$ neurons.**

**A**, Experimental design.

**B** and **C**, Traces (**B**) and qualifications (**C**) of THIP-induced currents in VTA GABA neurons and DA$_{NAc}$ neurons. n = 6–8 cells from 3 mice per group. Arrows in (**B**) indicate THIP-induced baseline shift. The concentration of THIP is 5 μM.

**D** and **E**, Traces (left) and quantifications (right) of cell-attached recordings from VTA GABA (**D**) and DA$_{NAc}$ neurons (**E**) in Gad2-mCherry mice before and after THIP (5 μM) application. GABA neurons: n = 19 cells from 5 mice per group. DA$_{NAc}$ neurons: n = 19 cells from 5 mice per group.

Data are reported as mean ± SEM. Student's t tests for **C**. Paired t tests for **D** and **E**. **p < 0.01, ***p < 0.001.

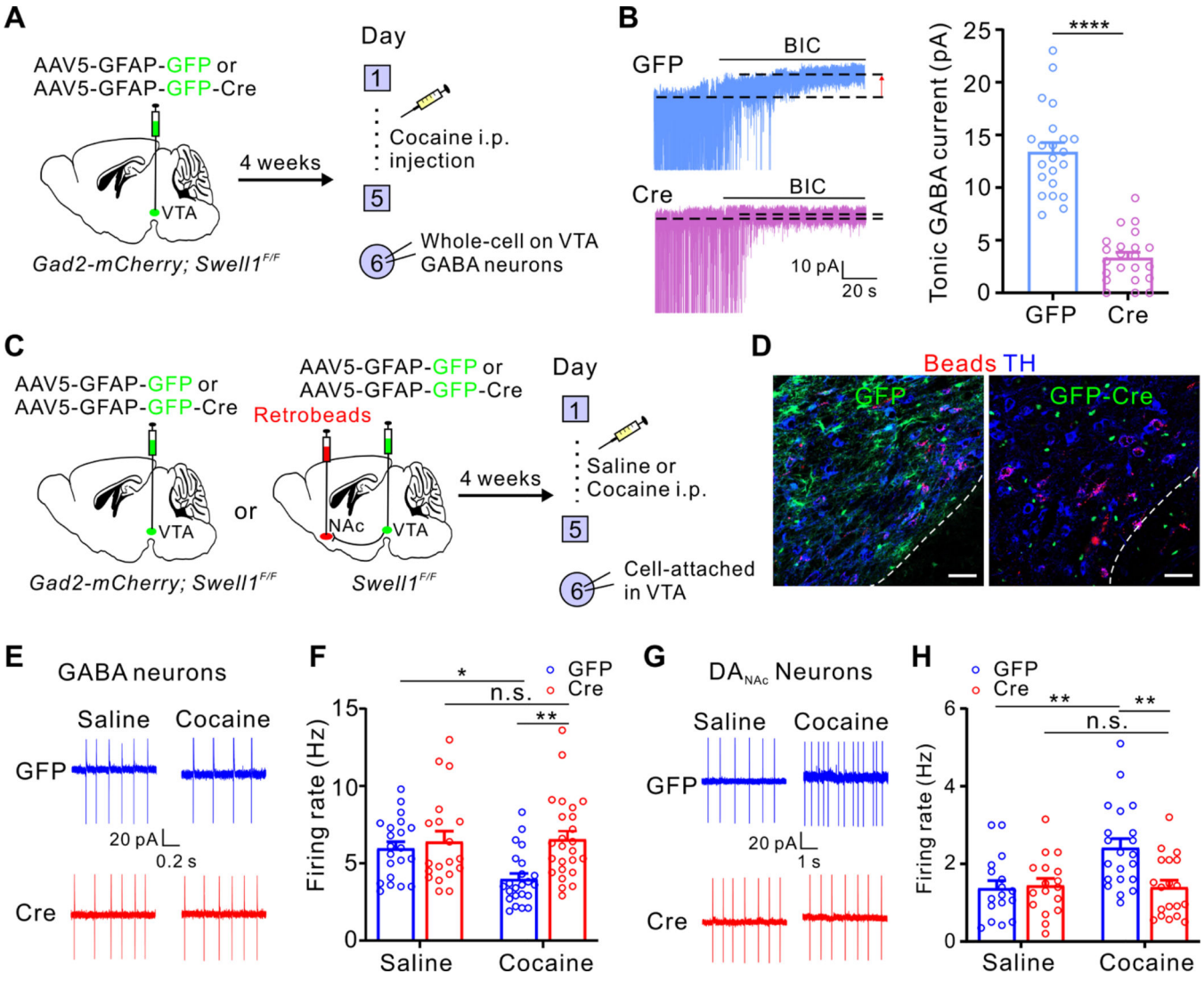


**Figure 5. *Swell1* deletion in VTA astrocytes reduces cocaine-induced changes in tonic inhibition and neuron firing.**

**A**, Experimental design.

**B**, Traces (left) and quantifications (right) of tonic inhibition current recordings from VTA GABA neurons of AAVs and cocaine-injected mice. n = 22 cells from 6 mice per group.

**C**, Scheme of the experimental protocol.

**D**, Confocal images showing the virus-infected VTA astrocytes and retrobead-labeled DA neurons. Scale bar, 40 μm.

**E-H,** Traces (**E, G**) and quantifications (**F, H**) of cell-attached recordings from VTA GABA (**E, F**) and DANAc neurons (**G, H**) in GFP and GFP-Cre-expressing mice injected with saline or cocaine. GABA neurons: n = 19–25 cells from 5–6 mice per group. $DA_{NAc}$ neurons: n = 17–21 cells from 5–6 mice per group.

Data are reported as mean ± SEM. Student's t tests for **B.** Two-way ANOVA, Bonferroni post hoc test for **F** and **H**. n.s., no significance. *p < 0.05, **p < 0.01, ****p < 0.0001

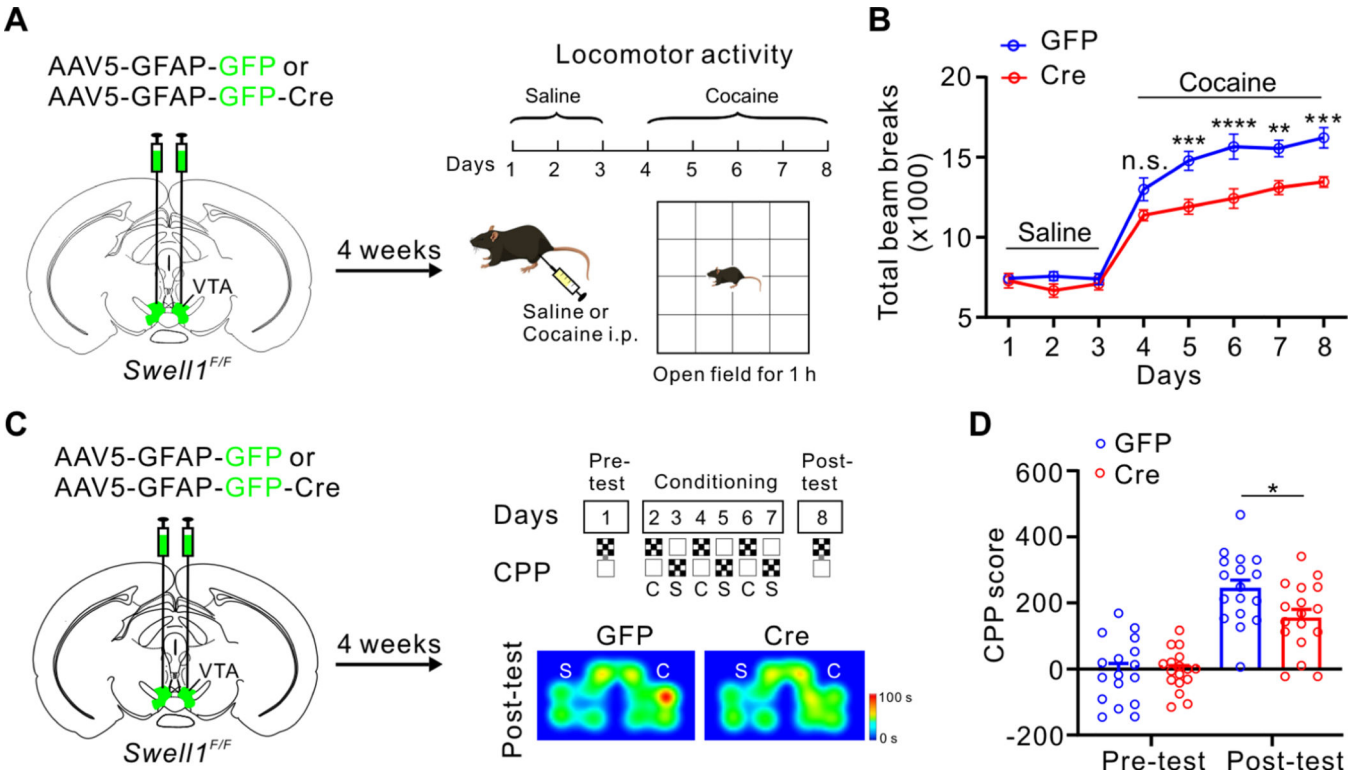


**Figure 6. *Swell1* deletion in VTA astrocytes attenuates cocaine addiction-related behaviors.**

**A**, Scheme of the experimental protocol. AAVs were bilaterally injected into VTA astrocytes and behavior was assessed 4 weeks later.

**B**, Locomotor activity, measured as infrared beam breaks, immediately after saline (days 1 to 3) or cocaine (15 mg/kg, days 4 to 8) injections. n = 15 mice (8 males and 7 females) for each group.

**C**, Scheme of the experimental protocol for CPP. AAVs were injected bilaterally into VTA, and behavior was assessed 4 weeks later. Baseline preference for each of the adjoining chambers was determined on day 1, referred to as the pre-conditioning test (Pre-test) day. Each experimental group was randomly divided into two subgroups. For one group, we paired cocaine (C, 10 mg/kg) with one chamber and paired saline (S) with the other chamber. For the other group, we reversed the pairings. The representative CPP heatmaps on the post-conditioning test (Post-test) day from GFP- and Cre-expressing mice are shown.

**D**, Quantification of CPP score. n = 17 (9 males and 8 females) mice for each group.

Data are reported as mean ± SEM. Two-way ANOVA, Bonferroni post hoc test for **B** and **D**. n.s., no significance. *p < 0.05, **p < 0.01, ***p < 0.001, ****p < 0.0001.

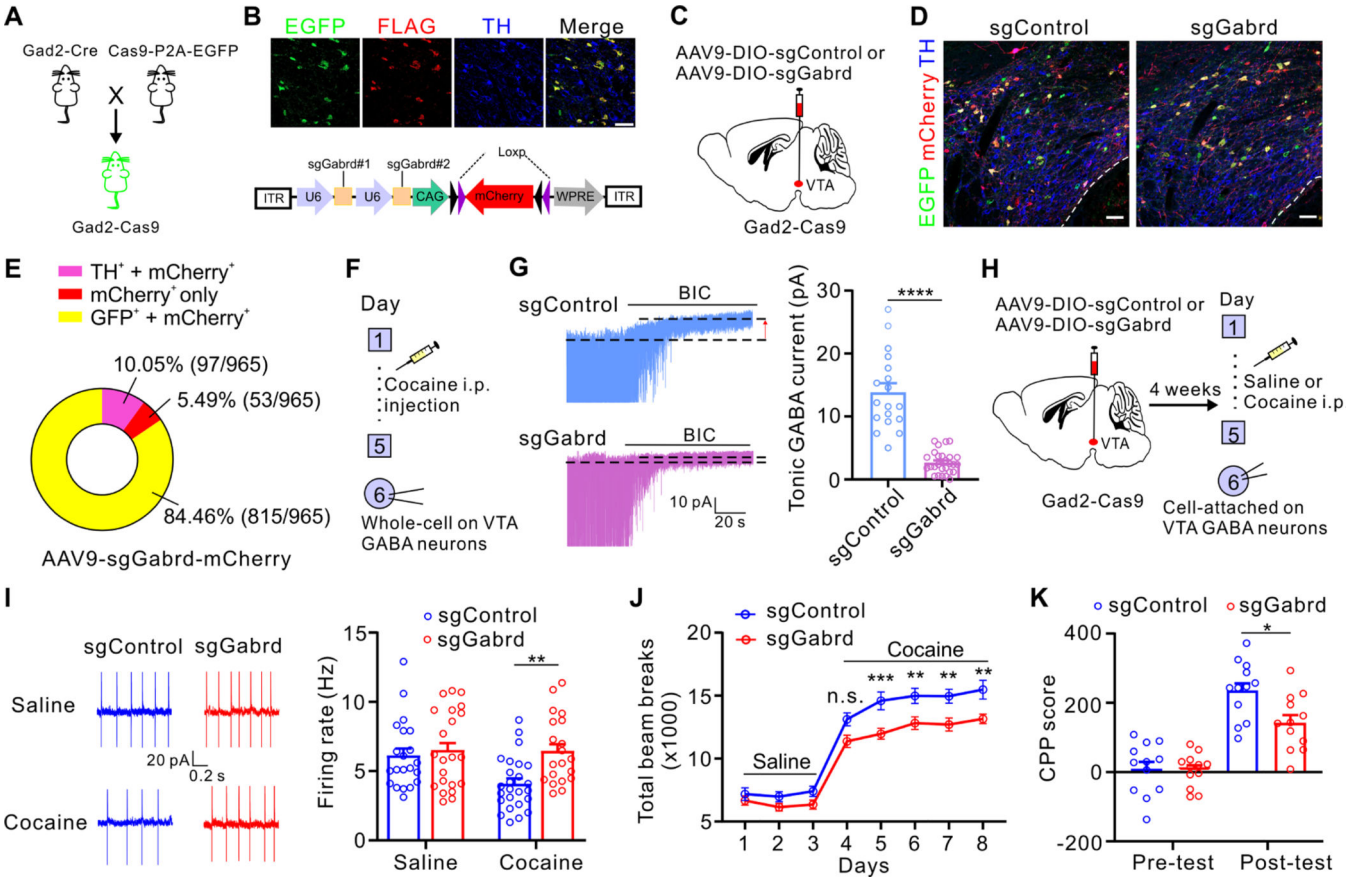


**Figure 7. Removal of tonic inhibition onto VTA GABA neurons rescues cocaine-induced electrophysiological and behavioral phenotypes.**

**A**, Design for expressing Cas9 in GABA neurons. A GABAergic inhibitory neuron driver line *Gad2-Cre* (*Gad2-IRES-Cre*) was crossed with the Cre-dependent Cas9 knock-in mice (LSL-Cas9–2A-EGFP).

**B**, Representative confocal images showing selective Cas9-FLAG expression in EGFP-positive VTA GABA neurons (top) and schematic of the AAV vector (bottom). Scale bar, 50 μm.

**C**, Schematic of AAV injection into VTA of Gad2-Cas9 mice.

**D**, Representative confocal images of the VTA from Gad2-Cas9 mice injected with AAV-sgControl or AAV-sgGabrd. Scale bar, 50 μm.

**E**, The pie charts show the quantification for (**D**). n = 965 neurons from 4 mice.

**F**, Experimental design.

**G**, Traces (left) and quantifications (right) of tonic inhibition current recordings from VTA GABA neurons in AAV and cocaine-injected mice. n = 20–27 cells from 5–6 mice per group.

**H**, Experimental design.

**I**, Traces (left) and quantifications (right) of cell-attached recordings from VTA GABA neurons in AAV-injected mice treated with saline or cocaine. n = 18–25 cells from 5–6 mice per group.

**J**, Quantification of locomotor activity after saline or cocaine injections. n = 14 mice (7 male and 7 female) per group.

**K**, Quantification of CPP score. n = 12 mice (6 male and 6 female) for each group.

Data are reported as mean ± SEM. Student's t tests for **G**. Two-way ANOVA, Bonferroni post hoc test for **I-K**. n.s., no significance. *p < 0.05, **p < 0.01, ***p < 0.001, ****p < 0.0001.

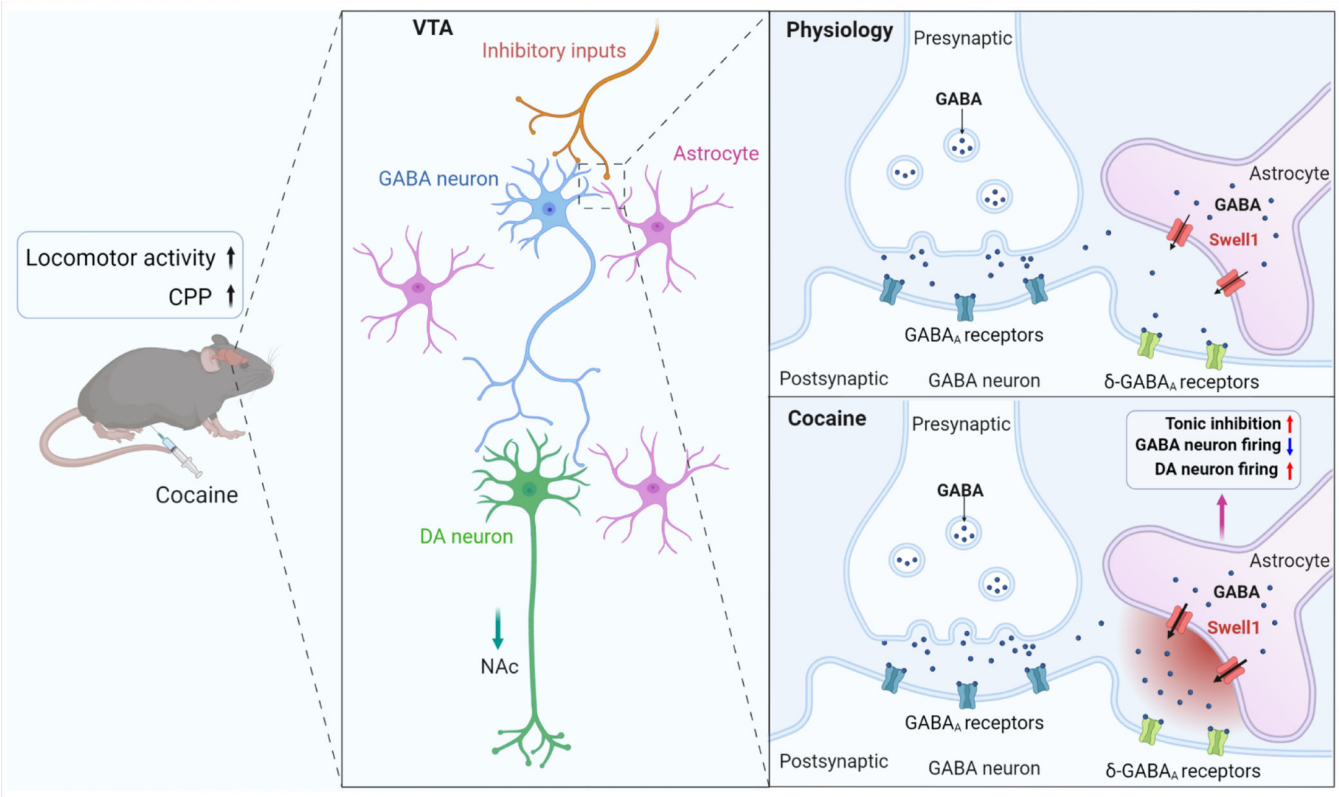


**Figure 8. Summary diagram.**

Swell1-mediated tonic GABA release from astrocytes contributes to the cellular and behavioral effects of cocaine in mice.

Key resources table

| REAGENT or RESOURCE | SOURCE | IDENTIFIER |
|---|---|---|
| Antibodies | | |
| Mouse monoclonal anti-GFAP (GA5 | Thermo Fisher Scientific | Cat# 14-989282; RRID: AB_10598206 |
| Mouse monoclonal anti-NeuN, clone A60 | Millipore | Cat# MAB377; RRID: AB_2298772 |
| Rabbit monoclonal anti-NeuN | Cell Signaling Technology | Cat# 24307; RRID: AB_2651140 |
| Rabbit polyclonal anti-GABA Transporter-3 | Millipore | Cat# AB1574; RRID: AB_90779 |
| Mouse monoclonal anti-TH | Millipore | Cat# MAB318; RRID: AB_ 2313764 |
| Rabbit polyclonal anti-TH | GeneTex | Cat# GTX113016; RRID: AB_1952230 |
| Rabbit polyclonal anti-S100β | Abcam | Cat# ab41548, RRID: AB_956280 |
| Rat anti-mCherry | Thermo Fisher Scientific | Cat# M11217; RRID: AB_2536611 |
| Rabbit anti-$GABA_{(A)}$ delta Receptor | Alomone Labs | Cat# AGA-014; RRID: AB_2340938 |
| Rabbit polyclonal anti-GFP | Thermo Fisher Scientific | Cat# A-11122; RRID: AB_221569 |
| Rat monoclonal anti-GFP | Nacalai Tesque | Cat# 04404–84; RRID: AB_10013361 |
| Mouse monoclonal anti-FLAG | Sigma-Aldrich | Cat# F1804; RRID: AB_262044 |
| Alexa Fluor 488 goat anti-rabbit | Thermo Fisher Scientific | Cat#A11008; RRID: AB_143165 |
| Alexa Fluor 488 goat anti-mouse | Thermo Fisher Scientific | Cat#A11029; RRID: AB_2534088 |
| Alexa Fluor 546 goat anti-mouse | Thermo Fisher Scientific | Cat# A11018; RRID: AB_1944229 |
| Alexa Fluor 546 goat anti-rabbit | Thermo Fisher Scientific | Cat# A11035; RRID: AB_2534093 |
| Alexa Fluor 546 goat anti-rat | Thermo Fisher Scientific | Cat# A11081; RRID: AB_2534125 |
| Alexa Fluor 647 goat anti-mouse | Thermo Fisher Scientific | Cat# A32728; RRID: AB_2633277 |
| Alexa Fluor 647 goat anti-rabbit | Thermo Fisher Scientific | Cat# A55055; RRID: AB_2921063 |
| Alexa Fluor 405-conjugated Streptavidin | Thermo Fisher Scientific | Cat# S32351; |
| Bacterial and virus strains | | |
| AAV5.GFAP.eGFP.WPRE.hGH | James M. Wilson lab | Addgene viral prep #105549-AAV5 |
| AAV5-GFAP-GFP-Cre | UNC vector core | https://www.med.unc.edu/genetherapy/vectorcore/in-stock-aav-vectors/ |
| AAV9-U6-sgGabrd#1-U6-sgGabrd#2-CAG-FLEX-mCherry | This study; WZ Biosciences | N/A |
| AAV9-U6-sgControl-U6-sgControl-CAG-FLEX-mCherry | This study; WZ Biosciences | N/A |
| Chemicals, peptides, and recombinant proteins | | |
| TTX | Hello bio | Cat# HB1035 |
| DL-APV | Sigma-Aldrich | Cat# A8054 |

| REAGENT or RESOURCE | SOURCE | IDENTIFIER |
|---|---|---|
| DNQX | Sigma-Aldrich | Cat# D0540 |
| Picrotoxin | Sigma-Aldrich | Cat# P1675 |
| Bicuculine | Sigma-Aldrich | Cat# 14340 |
| γ-aminobutyric acid (GABA) | Sigma Aldrich | Cat# A2129 |
| THIP | Sigma Aldrich | Cat# T101 |
| Paraformaldehyde | Sigma Aldrich | Cat# P1648 |
| Biocytin | Hello bio | Cat# HB5035 |
| Red retrobeads IX | Lumafluor | Item#: R170 |
| Green retrobeads IX | Lumafluor | Item#: G180 |
| RNAscope Multiplex Fluorescent Reagent Kit v.2 | Advanced Cell Diagnostics | Cat# 323100 |
| TSA Plus Fluorescence Kit | PerkinElmer | Cat# NEL741 Cat# NEL744 Cat# NEL745 |
| RNAscope® Probe-Mm-Lrrc8a | Advanced Cell Diagnostics | Cat# 458371 |
| Experimental models: Cell lines | | |
| Human: Human Embryonic Kidney (HEK) 293T cells | ATCC | Cat# CRL-3216 |
| Experimental models: Organisms/strains | | |
| Mouse: *mGFAP-cre (B6.Cg-Tg(Gfap-cre)77.6Mvs/2J* | The Jackson Laboratory | Stock#024098 RRID: IMSR_JAX:024098 |
| Mouse: *Swell1$^{flox}$* | Yang et al.[43] | N/A |
| Mouse: C57BL/6J | The Jackson Laboratory | Stock#000664 RRID: IMSR_JAX:000664 |
| Mouse: *Nestin-cre (B6.Cg-Tg(Nes-cre)1Kln/* | The Jackson Laboratory | Stock#003771 RRID: IMSR_JAX:003771 |
| Mouse: *Gad2-T2a-NLS-mCherry (B6;129S Gad2tm1.1Ksvo/J* | The Jackson Laboratory | Stock#023140 RRID: IMSR_JAX:023140 |
| Mouse: *Gad2-IRES-Cre (Gad2tm2(cre)Zjh/J* | The Jackson Laboratory | Stock#010802 RRID: IMSR_JAX:010802 |
| Mouse: *Rosa26-Cas9 knockin (Gt(ROSA)26Sortm1.1(CAG-cas9*,-EGFP)Fezh/J* | The Jackson Laboratory | Stock#024858 RRID: IMSR_JAX:024858 |
| Mouse: *Gabrd KO* | The Jackson Laboratory | Stock#003725 RRID: IMSR_JAX:003725 |
| Mouse: *Ai14 (B6;129S6-Gt(ROSA)26Sortm14(CAG-tdTomato)Hze/J* | The Jackson Laboratory | Stock#007908 RRID: IMSR_JAX:007908 |
| Oligonucleotides | | |
| sgGabrd#1 targeting sequence: 5′-TATGCCCGAAACTTCCGACCAGG-3′ | This paper | N/A |
| sgGabrd#2 targeting sequence: 5′-GGCCTAAGGTCTCGTTGGTATGG −3′ | This paper | N/A |
| Recombinant DNA | | |
| pIRES2-EGFP-Gabra6 | Wu et al.[36] | N/A |
| pCMV-Gabrb3 | Wu et al.[36] | N/A |
| pCMV-Gabrd | Wu et al.[36] | N/A |
| pAAV-U6-sgGabrd#1-U6-sgGabrd#2-CAG-FLEX-mCherry-WPRE | This paper | N/A |

| REAGENT or RESOURCE | SOURCE | IDENTIFIER |
|---|---|---|
| pAAV-U6-sgControl-U6-sgControl-CAG-FLEX-mCherry | This paper | N/A |
| Software and algorithms | | |
| pCLAMP 10.7 | Molecular Devices | http://www.moleculardevices.com/products/software/pclamp.html;RRID:SCR_011323 |
| Clampfit 10.7 | Molecular Devices | N/A |
| CorelDraw11 | Corel Corporation | https://www.coreldraw.com/en/;RRID:SCR_014235 |
| ImageJ | NIH | https://imagej.nih.gov/ij/download.html;RRID:SCR_003070 |
| GraphPad Prism 8 | GraphPad Software | https://www.graphpad.com/;RRID:SCR_002798 |
| ZEN 2.3 | ZEISS | https://www.zeiss.com/microscopy/en_us/products/microscope-software/zen.html#introduction;RRID:SCR_013672 |